THE JOURNAL OF BIOLOGICAL CHEMISTRY VOL. 291, NO. 33, pp. 17178–17196, August 12, 2016

Degradation of Serotonin *N*-Acetyltransferase, a Circadian Regulator, by the N-end Rule Pathway*

Received for publication, April 24, 2016, and in revised form, June 13, 2016 Published, JBC Papers in Press, June 23, 2016, DOI 10.1074/jbc.M116.734640

Brandon Wadas[‡], Jimo Borjigin[§], Zheping Huang[¶], Jang-Hyun Oh[‡], Cheol-Sang Hwang[‖], and Alexander Varshavsky[‡1]

From the [‡]Division of Biology and Biological Engineering, California Institute of Technology, Pasadena, California 91125, the [§]Department of Molecular and Integrative Physiology, University of Michigan Medical School, Ann Arbor, Michigan 48109, the [¶]Department of Immunology, University of Connecticut School of Medicine, Farmington, Connecticut 06030, and the [‖]Department of Life Sciences, Pohang University of Science and Technology, Pohang, Gyeongbuk, 790-784, South Korea

Serotonin *N*-acetyltransferase (AANAT) converts serotonin to *N*-acetylserotonin (NAS), a distinct biological regulator and the immediate precursor of melatonin, a circulating hormone that influences circadian processes, including sleep. N-terminal sequences of AANAT enzymes vary among vertebrates. Mechanisms that regulate the levels of AANAT are incompletely understood. Previous findings were consistent with the possibility that AANAT may be controlled through its degradation by the N-end rule pathway. By expressing the rat and human AANATs and their mutants not only in mammalian cells but also in the yeast *Saccharomyces cerevisiae*, and by taking advantage of yeast genetics, we show here that two "complementary" forms of rat AANAT are targeted for degradation by two "complementary" branches of the N-end rule pathway. Specifically, the N$^{\alpha}$-terminally acetylated (Nt-acetylated) Ac-AANAT is destroyed through the recognition of its Nt-acetylated N-terminal Met residue by the Ac/N-end rule pathway, whereas the non-Nt-acetylated AANAT is targeted by the Arg/N-end rule pathway, which recognizes the unacetylated N-terminal Met-Leu sequence of rat AANAT. We also show, by constructing lysine-to-arginine mutants of rat AANAT, that its degradation is mediated by polyubiquitylation of its Lys residue(s). Human AANAT, whose N-terminal sequence differs from that of rodent AANATs, is longer-lived than its rat counterpart and appears to be refractory to degradation by the N-end rule pathway. Together, these and related results indicate both a major involvement of the N-end rule pathway in the control of rodent AANATs and substantial differences in the regulation of rodent and human AANATs that stem from differences in their N-terminal sequences.

Arylalkylamine *N*-acetyltransferase (AANAT)[2] converts the neurotransmitter serotonin to *N*-acetylserotonin (NAS) (1–11). Regulatory functions of NAS include its activity as an agonist of TrkB, the receptor for the brain-derived neurotrophic factor (12–14). NAS is the immediate precursor of melatonin, a circulating hormone that regulates sleep and other circadian processes in vertebrates. Melatonin is also present in invertebrates, including insects, as well as in animals that lack recognizable neurons (1, 15–21). The functions of melatonin in mammals include the modulation of circadian rhythms in response to light-dark cycles. Melatonin also contributes to the control of seasonal physiology (20). These mechanisms are a part of a broader range of processes that involve distinct biological oscillators in all organisms (22–24). In the course of daily light-dark cycles, the activity of AANAT and the level of the ~23-kDa AANAT protein in the brain's pineal gland are high during nocturnal periods and rapidly decrease following exposure to light (1, 20, 25).

In mammals, changes of AANAT levels in the brain's pineal gland are controlled by the circadian oscillator in the suprachiasmatic nucleus of the hypothalamus. At night, axons of rodent superior cervical ganglion neurons release norepinephrine in the pineal gland, in response to circadian signals from the suprachiasmatic nucleus, thereby activating adrenergic receptors to increase intracellular Ca^{2+} and cAMP. The resulting phosphorylation of CREB, the cAMP-response element-binding protein, up-regulates the *Aanat* transcriptional promoter, which contains cAMP-response element sequence elements (1, 4, 25–27). Increases in cAMP also stimulate the site-specific phosphorylation of AANAT by PKA, thereby causing the binding of AANAT to 14-3-3 proteins. These transitions augment the enzymatic activity of AANAT and inhibit its degradation (1, 6, 7, 28). Although AANAT is predominantly expressed in the pineal gland and the retina, this enzyme is also present in cells of the gastrointestinal tract and apparently at other sites as well, including the hippocampus, the olfactory bulb, the cerebellum, and the spinal cord (12, 29, 30).

Melatonin is produced from NAS by hydroxyindole-*O*-methyltransferase. The levels of NAS, synthesized by AANAT, can constrain the rate of melatonin synthesis from NAS during light parts of daily cycles (when NAS levels are low) but appear

* This study was supported by National Institutes of Health Grants R01-DK039520 and R01-GM031530 (to A. V.) and R01-NS057583 (to J. B.). The authors declare that they have no conflicts of interest with the contents of this article. The content is solely the responsibility of the authors and does not necessarily represent the official views of the National Institutes of Health.

[1] To whom correspondence should be addressed. E-mail: avarsh@caltech.edu.

[2] The abbreviations used are: AANAT, arylalkylamine *N*-acetyltransferase; Ub, ubiquitin; NAS, *N*-acetylserotonin; CHX, cycloheximide; N-degron, an N-terminal degradation signal recognized by the N-end rule pathway; N-recognin, an E3 ubiquitin ligase that can recognize at least some N-degrons; CREB, cAMP-response element-binding protein; Nt-, N$^{\alpha}$-terminally/N$^{\alpha}$-terminal; MetAP, Met-aminopeptidase; LDS, lithium dodecyl sulfate; BisTris, 2-[bis(2-hydroxyethyl)amino]-2-(hydroxymethyl)propane-1,3-diol.

not to be the rate-limiting step during dark parts of these cycles, when both AANAT and NAS levels are high (21). In rodents such as rats, the activity of AANAT starts to increase 3–4 h after the onset of darkness and begins to decrease before the onset of light in the morning (21, 31). Hence the importance of regulating the expression and the enzymatic activity of AANAT, because these parameters determine the levels of both NAS and melatonin.

The concentration of AANAT, a largely cytosolic enzyme (32), is controlled through both transcriptional and post-translational mechanisms (1, 11, 31, 33–35). In rodents, the onset of darkness leads to an increase in melatonin (requiring a preceding increase of NAS) after a lag period, whereas in sheep and primates, increases in melatonin occur rapidly upon the onset of darkness. The levels of *Aanat* mRNA in rodents can vary by >100-fold during light-dark cycles (10), whereas in non-rodent mammals such as, for example, sheep, these differences can be as low as ~2-fold, suggesting a major involvement of translational and/or post-translational AANAT regulation in latter cases (11, 36). In addition to variability in regulation at the level of AANAT-encoding mRNAs, AANAT is also unusual in the extent of variability of its N-terminal sequences during vertebrate evolution (Fig. 1*C*). In 2010, one of our laboratories showed that N-terminal residues of rat AANAT play a role in the control of its degradation, suggesting the involvement of the N-end rule pathway (37).

The N-end rule pathway is a set of intracellular proteolytic systems whose unifying feature is the ability to recognize and polyubiquitylate proteins containing N-terminal degradation signals (degrons) called N-degrons, thereby causing degradation of these proteins by the proteasome (Fig. 1, *A* and *B*) (38–46). Ubiquitin (Ub) ligases of the N-end rule pathway, called N-recognins, can recognize not only N-degrons but also specific internal degradation signals (47–50). The main determinant of an N-degron is either an unmodified or chemically modified destabilizing N-terminal residue of a protein. Another determinant of an N-degron is a protein's internal Lys residue(s). It functions as the site of polyubiquitylation and tends to be located in a conformationally disordered region (41, 51, 52). Bacteria also contain the N-end rule pathway, but Ub-independent versions of it (53–58).

Regulated degradation of proteins and their natural fragments by the N-end rule pathway has been shown to mediate a strikingly broad range of biological functions, including the sensing of heme, nitric oxide (NO), oxygen, and short peptides; the control of the input stoichiometries of subunits in oligomeric protein complexes; the elimination of misfolded or otherwise abnormal proteins; the degradation of specific proteins after their retrotranslocation to the cytosol from membrane-enclosed compartments; the regulation of apoptosis and repression of neurodegeneration; the regulation of DNA repair, transcription, replication, and chromosome cohesion/segregation; the regulation of G proteins and cytoskeletal proteins, such as actin and myosin; the regulation of autophagy, peptide import, meiosis, immunity, fat metabolism, cell migration, cardiovascular development, spermatogenesis, and neurogenesis; the functioning of adult organs, including the brain, muscle, testis, and pancreas; and the regulation of leaf and shoot development, leaf senescence, and many other processes in plants (Fig. 1, *A* and *B*) (see Refs. 41–46 and references therein).

In eukaryotes, the N-end rule pathway consists of two branches. One branch, called the Ac/N-end rule pathway, targets proteins for degradation through their N^{α}-terminally acetylated (Nt-acetylated) residues (Fig. 1*B*) (39, 40, 46, 59–62). Degradation signals and E3 Ub ligases of the Ac/N-end rule pathway are called Ac/N-degrons and Ac/N-recognins, respectively. Nt-acetylation of cellular proteins is apparently irreversible, in contrast to acetylation-deacetylation of proteins' internal Lys residues. About 90% of human proteins are cotranslationally Nt-acetylated by ribosome-associated Nt-acetylases (63). Ac/N-degrons are present in many, possibly most, Nt-acetylated proteins (Fig. 1*B*). Natural Ac/N-degrons are regulated through their reversible shielding in cognate protein complexes (59).

The pathway's other branch, called the Arg/N-end rule pathway, targets specific unacetylated N-terminal residues (Fig. 1*A*) (40, 64–68). The "primary" destabilizing N-terminal residues Arg, Lys, His, Leu, Phe, Tyr, Trp, and Ile are directly recognized by N-recognins. The unacetylated N-terminal Met, if it is followed by a bulky hydrophobic (Φ) residue, also acts as a primary destabilizing residue (Fig. 1*A*) (40). In contrast, the unacetylated N-terminal Asn, Gln, Asp, and Glu (as well as Cys, under some metabolic conditions) are destabilizing due to their preliminary enzymatic modifications, which include N-terminal arginylation (Fig. 1*A*) (41–43, 69). In the yeast *Saccharomyces cerevisiae*, the Arg/N-end rule pathway is mediated by the Ubr1 N-recognin, a 225-kDa RING-type E3 Ub ligase and a part of the targeting complex comprising the Ubr1-Rad6 and Ufd4-Ubc4/5 E2-E3 holoenzymes (41, 70). In multicellular eukaryotes, several E3 Ub ligases, including Ubr1, function as N-recognins of the Arg/N-end rule pathway (Fig. 1*A*).

In *S. cerevisiae*, the Ac/N-end rule pathway is mediated by (at least) the cytosolic/nuclear E3 Ub ligase Not4 and by Doa10, an endoplasmic reticulum membrane-embedded E3 (59). In mammalian cells, this pathway is mediated by (at least) the Teb4 E3, which is sequelogous (similar in sequence (71)) to yeast Doa10 (60). Human RGS2, a regulator of specific G proteins, is a short-lived substrate of the Ac/N-end rule pathway both in mammalian cells and in the heterologous setting of *S. cerevisiae* (60, 72, 73). In addition, the naturally occurring (blood pressure-elevating) human $RGS2^{Q2L}$ mutant (in which Gln at position 2 is replaced by Leu) is targeted for degradation by both the Ac/N-end rule pathway and the Arg/N-end rule pathway (60). The Ac/N-end rule pathway recognizes the Nt-acetylated Ac-$RGS2^{Q2L}$ (specifically its N-terminal Ac-Met residue), whereas the non-Nt-acetylated $RGS2^{Q2L}$ is targeted (through its N-terminal Met-Leu sequence) by the Arg/N-end rule pathway (60).

In the present work, we analyzed the proteasome-mediated degradation of rat AANAT (37), whose N-terminal sequence Met-Leu (Fig. 1*C*) is identical to that of the otherwise unrelated human $RGS2^{Q2L}$ protein (60). We also characterized human AANAT, which is highly sequelogous (71) (84% identical) to rat AANAT but bears a different N-terminal sequence (Fig. 1*C*). Our analyses employed the previously helpful approach of dissecting degradation of a mammalian protein of interest not only

in a homologous (mammalian) setting but also in *S. cerevisiae* (60, 66), thereby making possible the use of yeast genetics.

We show here that two alternative versions of rat AANAT, its Nt-acetylated and non-Nt-acetylated forms, are targeted for degradation by the Ac/N-end rule pathway and the Arg/N-end rule pathway, respectively. In contrast, human AANAT, whose N-terminal sequence differs from that of rodent AANATs, is significantly longer-lived than its rat counterpart and appears to be largely refractory to degradation by the N-end rule pathway. Together, these and related results indicate both a major involvement of the N-end rule pathway in the control of rodent AANATs and substantial differences in the regulation of rodent and human AANATs that stem from differences in their N-terminal sequences.

Results

Wild-type Rat and Human AANATs and Their Mutants—The start (AUG) codon-encoded N-terminal Met residue of nascent proteins is cotranslationally cleaved off by ribosome-associated Met-aminopeptidases (MetAPs) if a residue at position 2, to be made N-terminal by the cleavage, is not larger than Val (41, 74). Thus, for example, the Met residue of the N-terminal Met-Leu-Ser sequence of wild-type rat AANAT (denoted as ^{MLS}rAANAT) (Fig. 1*C*) is retained in mature ^{MLS}rAANAT, inasmuch as Leu is larger than Val. Given the previously demonstrated usefulness of employing genetic tractability of *S. cerevisiae* for understanding the targeting of mammalian N-end rule substrates (60, 66), we carried out the present study by expressing AANAT test proteins not only in human HEK293T cells but also in *S. cerevisiae*. Cited below are the examined wild-type and mutant AANAT proteins.

When present, parentheses around a superscript's N-terminal Met residue in the notations of AANAT test proteins denote the fact that this Met is cotranslationally cleaved off by MetAPs.

(i) ^{MLS}rAANAT$_{3f}$, the wild-type rat ^{MLS}rAANAT C-terminally tagged with a triple-FLAG epitope (Figs. 1*C* and 2*A*).

(ii) $^{(M)SMLS}$rAANAT$_{3f}$, in which the sequence (Met)-Ser was placed before the wild-type Met-Leu-Ser sequence of rat ^{MLS}rAANAT$_{3f}$, yielding the N-terminal sequence (Met)-Ser-Met-Leu-Ser. Its N-terminal Met residue would be cotranslationally cleaved off by MetAPs (Fig. 2*A*). The (Met)-Ser sequence was added to wild-type ^{MLS}rAANAT$_{3f}$ in order to mimic the (Met)-Ser N-terminal sequence of primate (including human) AANATs (Fig. 1*C*).

(iii) $^{(M)SI}$rAANAT$_{3f}$, in which Leu at position 2 of the wild-type rat ^{MLS}rAANAT$_{3f}$ (Fig. 1*C*) was deleted, thereby making the N-terminal Met of the resulting $^{(M)SI}$rAANAT$_{3f}$ removable by MetAPs (Figs. 1*C* and 2*A*).

(iv) $^{(M)PLS}$rAANAT$_{3f}$, in which the Pro residue was inserted between N-terminal Met and second-position Leu of wild-type rat ^{MLS}rAANAT$_{3f}$. This alteration aimed to address the relevance of Nt-acetylation to the degradation of wild-type rat ^{MLS}rAANAT$_{3f}$. Specifically, the N-terminal sequence Met-Leu-Ser is *a priori* likely to be cotranslationally Nt-acetylated *in vivo* at its (retained) N-terminal Met (59, 62, 63). In contrast, the N-terminal Met residue of the mutant N-terminal sequence (Met)-Pro-Leu-Ser of $^{(M)PLS}$rAANAT$_{3f}$ would be cotranslationally cleaved off by MetAPs. The resulting N-terminal Pro is not Nt-acetylated, at least in *S. cerevisiae*, and is usually not Nt-acetylated in mammalian cells as well (59, 63).

(v) ^{MLS}rAANAT$_{3ha}$, the wild-type rat ^{MLS}rAANAT (Fig. 1*C*) C-terminally tagged with a triple-HA epitope. It was used as a control for the ^{MLS}rAANAT$^{K8R}_{3ha}$ mutant described in item viii.

(vi) $^{(M)ST}$hAANAT$_{3f}$, the wild-type human $^{(M)ST}$hAANAT (Fig. 1*C*) C-terminally tagged with a triple-FLAG epitope.

(vii) $^{(M)PT}$hAANAT$_{3f}$, in which the second-position Ser of the wild-type human $^{(M)ST}$hAANAT$_{3f}$ (Fig. 1*C*) was replaced by the Pro residue, yielding $^{(M)PT}$hAANAT$_{3f}$. The N-terminal Met residue of either the wild-type human $^{(M)ST}$hAANAT$_{3f}$ or the mutant $^{(M)PT}$hAANAT$_{3f}$ would be cotranslationally removed by MetAPs (41, 74). However, in contrast to the resulting N-terminal Ser of wild-type SThAANAT$_{3f}$, which would be expected to be cotranslationally Nt-acetylated, the N-terminal Pro of the mutant ^{PT}hAANAT$_{3f}$ is not Nt-acetylated, at least in *S. cerevisiae*, and is usually not Nt-acetylated in mammalian cells as well (59, 63).

(viii) ^{MLS}rAANAT$^{K8R}_{3ha}$, the otherwise wild-type triple-HA-tagged rat ^{MLS}rAANAT in which the Lys-8 residue was replaced by Arg.

(ix) ^{MLS}rAANAT$^{Kzero}_{3ha}$, the otherwise wild-type triple-HA-tagged rat ^{MLS}rAANAT in which each of its four Lys residues were replaced by Arg (Fig. 6*B*).

(x) $^{(M)ST}$hAANAT$^{Kzero}_{3ha}$, the otherwise wild-type triple-HA-tagged human $^{(M)ST}$hAANAT in which both of its Lys residues were replaced by Arg (Fig. 7, *A* and *D*).

Degradation of Rat AANAT by the S. cerevisiae N-end Rule Pathway—In cycloheximide (CHX) assays, a protein of interest is analyzed by immunoblotting as a function of time after the inhibition of translation by CHX (39, 59, 60). Both the wild-type rat ^{MLS}rAANAT$_{3f}$ (Fig. 1*C*) and its $^{(M)SMLS}$rAANAT$_{3f}$ mutant (see item ii above) were rapidly degraded in wild-type *S. cerevisiae*, with half-lives ($t_{½}$) $<$ 5 min (Fig. 2, *B* (*lanes 3–10*) and *D*). In striking contrast, $^{(M)SI}$rAANAT$_{3f}$ (see item iii above), produced from wild-type ^{MLS}rAANAT$_{3f}$ by deleting the Leu residue at position 2, was virtually completely stable under the same conditions, with a $t_{½} > 1$ h (Fig. 2, *B* (*lanes 11–14*) and *D*).

Because the N-terminal Met residue in the Met-Leu-Ser sequence of the wild-type rat ^{MLS}rAANAT$_{3f}$ would be likely to be Nt-acetylated *in vivo* (59, 62, 63), the rapid degradation of ^{MLS}rAANAT$_{3f}$ ($t_{½} <$ 5 min) (Fig. 2, *B* and *D*) suggested the involvement of the Ac/N-end rule pathway (Fig. 1*A*). To address this possibility, we constructed the non-Nt-acetylatable $^{(M)PLS}$rAANAT$_{3f}$ mutant (see item iv above). (This mutant would also not be expected to be targetable by the Arg/N-end rule pathway, because the latter does not recognize N-terminal Pro (40, 41).) Remarkably, $^{(M)PLS}$rAANAT$_{3f}$ was long-lived in *S. cerevisiae*, in comparison with the short-lived wild-type ^{MLS}rAANAT$_{3f}$ ($t_{½} \approx$ 1 h *versus* $t_{½} <$ 5 min, respectively), strongly suggesting (but not proving) a role for the Ac/N-end rule pathway in the degradation of the wild-type rat ^{MLS}rAANAT$_{3f}$ (Fig. 2, *B* (*lanes 15–18*) and *D*; also see below).

To further address the involvement of the Ac/N-end rule and Arg/N-end rule pathways (Fig. 1, *A* and *B*) in the degradation of wild-type ^{MLS}rAANAT$_{3f}$, we performed CHX-chases in *S. cerevisiae* mutants that lacked essential components of either

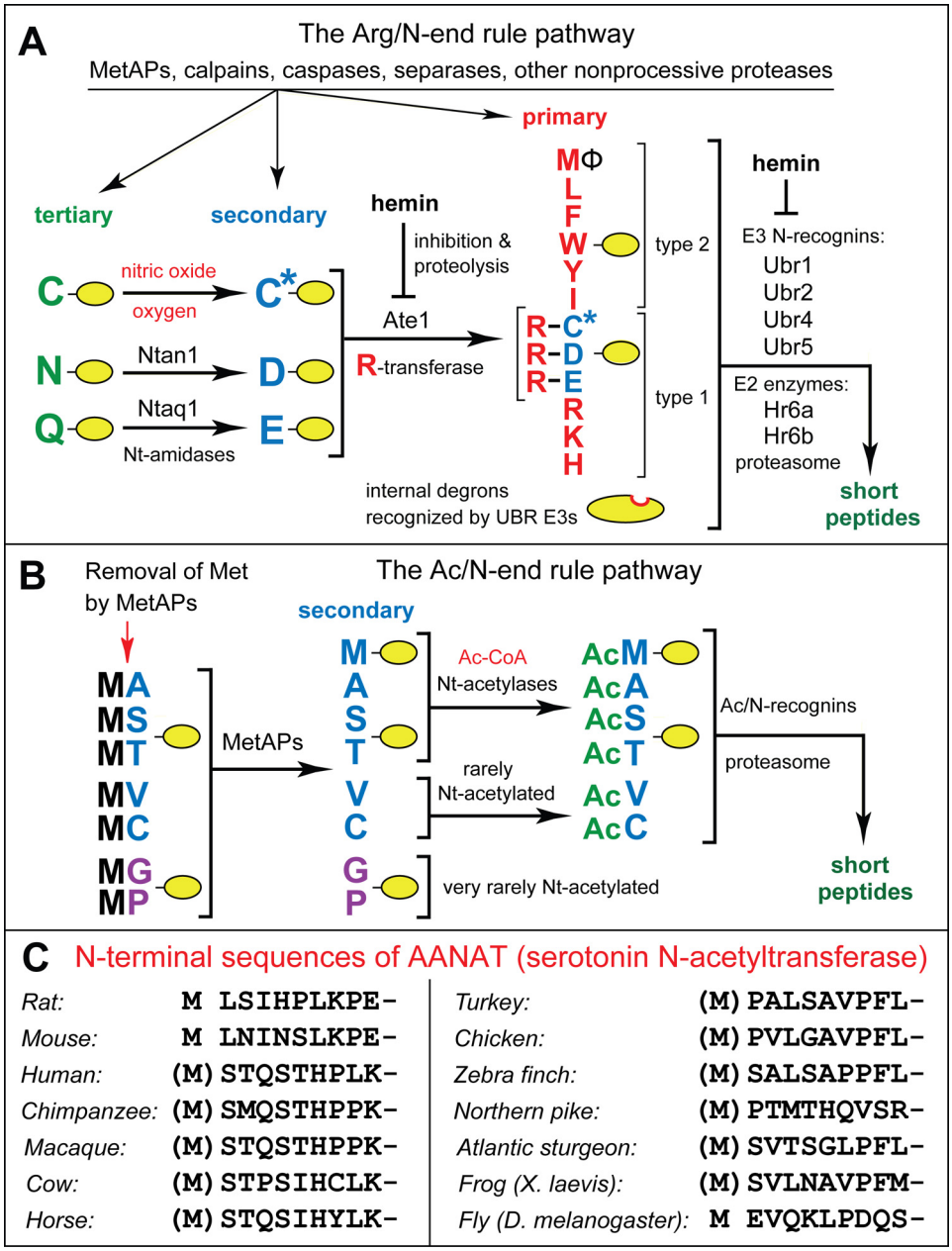

FIGURE 1. **The mammalian N-end rule pathway and N-terminal regions of AANAT enzymes.** See the Introduction for references and descriptions of the pathway's mechanisms and biological functions. Amino acid residues are denoted by *single-letter codes*. *A*, the mammalian Arg/N-end rule pathway. It targets proteins for degradation through their specific unacetylated N-terminal residues. A *yellow oval* denotes the rest of a protein substrate. *Primary*, *secondary*, and *tertiary*, mechanistically distinct classes of destabilizing N-terminal residues. *Ntan1* and *Ntaq1*, N-terminal amidases (*Nt-amidases*) that convert the tertiary destabilizing N-terminal residues Asn and Gln to Asp and Glu, respectively. The Ate1 arginyltransferase (*R-transferase*) conjugates Arg, a primary destabilizing residue, to N-terminal Asp, Glu, and (oxidized) Cys. *Type 1* and *type 2*, two sets of primary destabilizing N-terminal residues, basic (Arg, Lys, and His) and bulky hydrophobic (Leu, Phe, Trp, Tyr, Ile, and Met, if the latter is followed by a bulky hydrophobic residue (Φ)), respectively. These sets of N-terminal residues are recognized by two distinct substrate-binding sites of N-recognins, the pathway's E3 ubiquitin ligases, whose (possibly incomplete) list includes Ubr1, Ubr2, Ubr4, and Ubr5. *B*, mammalian Ac/N-end rule pathway. It targets proteins through their N^{α}-terminally acetylated (*Nt-acetylated*) residues. *Red arrow* on the *left*, cotranslational removal of the N-terminal Met residue by Met-aminopeptidases (*MetAPs*). N-terminal Met is retained if a residue at position 2 is larger than Val. *C*, the first 10 amino acid residues of animal AANAT enzymes, in vertebrates and an invertebrate, such as *Drosophila melanogaster*. See the Introduction for descriptions of AANATs.

one or both of these pathways. The normally short-lived rat ^{MLS}rAANAT$_{3f}$ ($t_{½} < 5$ min; Fig. 2, *C* (*lanes 2–5*) and *E*) was partially stabilized in both *naa30*Δ and *ubr1*Δ mutants (Fig. 2, *C* (*lanes 6–9* and *14–17*) and *E*). *S. cerevisiae naa30*Δ cells lack the cognate NatC Nt-acetylase whose substrates include proteins bearing the N-terminal Met-Leu sequence (59, 62, 63, 75, 76). *S. cerevisiae ubr1*Δ cells lack Ubr1, the E3 Ub ligase (N-recognin) that is essential for the proteolytic activity of the Arg/N-end rule pathway (Fig. 1*A*) (40, 41, 59).

Crucially, the relative stabilization of ^{MLS}rAANAT$_{3f}$ was dramatically higher in the double mutant *naa30*Δ *ubr1*Δ than in either one of the single mutants (Fig. 2, *C* (*lanes* 18–21) and *E*). These findings should be considered together with the conceptually independent result that the non-Nt-acetylatable (and

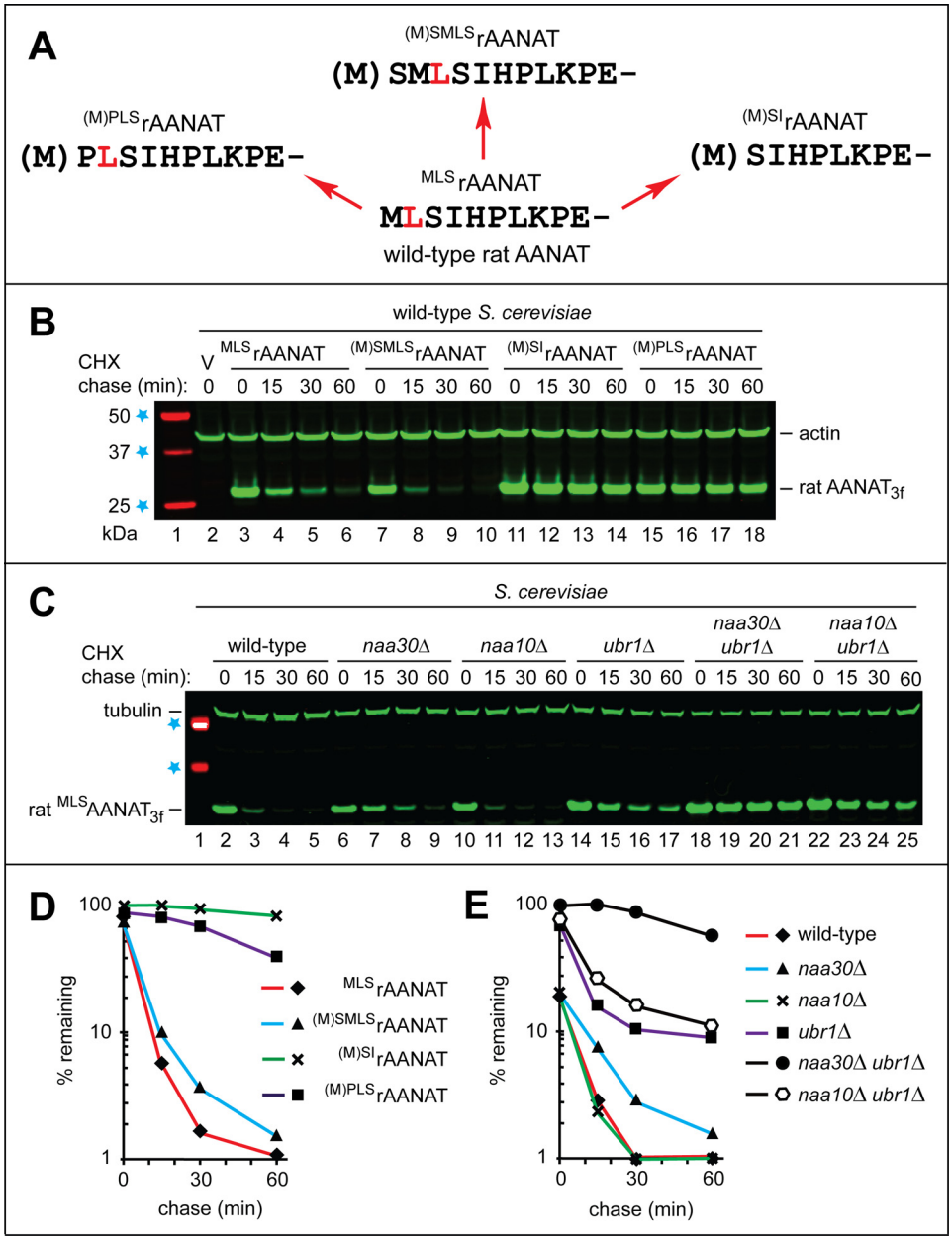

FIGURE 2. **The wild-type rat ^{MLS}rAANAT as a substrate of both branches of the N-end rule pathway.** *A*, the wild-type rat ^{MLS}rAANAT and its mutants that were constructed and analyzed in the present study. Amino acid residues are denoted by *single-letter codes*. The Leu residue, at position 2 in wild-type ^{MLS}rAANAT, is *highlighted* in *red* to make it easier to follow sequence alterations in specific mutants. *B*, immunoblotting with antibody to actin was used as a loading control. *Lane 1*, fluorescently labeled molecular mass markers (LI-COR); their masses, in kDa, are indicated on the *left*. *Lane 2*, wild-type *S. cerevisiae* were transformed with vector (*V*) alone (control). CHX-chases were performed at 30 °C for the indicated times in wild-type *S. cerevisiae* with the wild-type rat ^{MLS}rAANAT$_{3f}$ (*lanes 3–6*) and with its mutants $^{(M)SMLS}$rAANAT$_{3f}$ (*lanes 7–10*), $^{(M)SI}$rAANAT$_{3f}$ (*lanes 11–14*), and $^{(M)PLS}$rAANAT$_{3f}$ (*lanes 15–18*). The bands of AANAT$_{3f}$ and actin are indicated on the *right*. *C*, immunoblotting with antibody to tubulin was used as a loading control. *Lane 1*, 37 and 50 kDa molecular mass markers (see *lane 1* in *B*). Shown are CHX-chases with the wild-type rat ^{MLS}rAANAT$_{3f}$ in wild-type *S. cerevisiae* (*lanes 2–5*) and its mutants *naa30*Δ (*lanes 6–9*), *naa10*Δ (*lanes 10–13*), *ubr1*Δ (*lanes 14–17*), *naa30*Δ *ubr1*Δ (*lanes 18–21*), and *naa10*Δ *ubr1*Δ (*lanes 22–25*). The bands of ^{MLS}rAANAT$_{3f}$ and tubulin are indicated on the left. *D*, quantification of data in *B*. *E*, quantification of data in *C*. All quantified CHX-chase assays were carried out at least three times and yielded results within 10% of the data shown.

also not targetable by the Arg/N-end rule pathway) $^{(M)PLS}$rAANAT$_{3f}$ mutant (see the preceding paragraph) was much longer-lived in wild-type *S. cerevisiae* than its wild-type ^{MLS}rAANAT$_{3f}$ counterpart (Fig. 2, *B* (*lanes 15–18 versus lanes 3–6*) and *D*). Together, these sets of findings indicated that the wild-type rat ^{MLS}rAANAT$_{3f}$ (its two alternative forms) was targeted for degradation by both the Ac/N-end rule pathway and the Arg/N-end rule pathway. Specifically, the Nt-acetylated Ac-^{MLS}rAANAT$_{3f}$ is destroyed through the recognition of its Nt-acetylated N-terminal Met residue by the Ac/N-end rule pathway (Fig. 1*B*), whereas the non-Nt-acetylated ^{MLS}rAANAT$_{3f}$ is targeted by the "complementary" Arg/N-end rule pathway, which recognizes the unacetylated N-terminal Met-Leu sequence of ^{MLS}rAANAT$_{3f}$ as the Met-Φ motif (N-terminal Met followed by a bulky hydrophobic residue) (Fig. 1*A*).

This conclusion was in agreement with the finding that the rapid degradation of ^{MLS}rAANAT$_{3f}$ in wild-type *S. cerevisiae*

($t_{1/2} < 5$ min) remained unchanged in *naa10*Δ cells, which lacked the non-cognate NatA Nt-acetylase (which does not Nt-acetylate N-terminal Met) (59, 76). Furthermore and also in agreement with the above conclusion, the degradation of ^{MLS}rAANAT$_{3f}$ in double-mutant *naa10*Δ *ubr1*Δ cells proceeded at a rate similar to that in the single *ubr1*Δ mutant (Fig. 2, *C* (*lanes 22–25*) and *E*). Thus, a double-mutant background that nearly completely stabilizes the wild-type rat ^{MLS}rAANAT$_{3f}$ must be *naa30*Δ *ubr1*Δ in that it should also lack the activity of the cognate NatC Nt-acetylase (Fig. 2, *C* (*lanes 18–21*) and *E*). In agreement with this conclusion, the ablation of *NAA10*, encoding the non-cognate NatA Nt-acetylase, did not have a synergistic effect on the rate of ^{MLS}rAANAT$_{3f}$ degradation in double-mutant *naa10*Δ *ubr1*Δ cells (Fig. 2, *C* (*lanes 22–25*) and *E*).

Previous work has identified the endoplasmic reticulum membrane-embedded E3 Ub ligase Doa10 as one Ac/N-recognin of the *S. cerevisiae* Ac/N-end rule pathway (39, 59). We found that the degradation of the wild-type rat ^{MLS}rAANAT$_{3f}$ ($t_{1/2} < 5$ min in wild-type *S. cerevisiae*) was not significantly impaired in *doa10*Δ cells, in comparison with wild-type cells (Fig. 3, *D* and *F*). We did not examine, so far, the other yeast Ac/N-recognin, Not4 (see the Introduction) for its possible role in targeting the Nt-acetylated rat Ac-^{MLS}rAANAT$_{3f}$ in *S. cerevisiae*. We also do not know, thus far, whether Teb4, the mammalian counterpart of the yeast Doa10 Ac/N-recognin (60), is involved in the degradation of rat ^{MLS}rAANAT$_{3f}$ in a homologous (mammalian) setting.

Degradation of Rat AANAT Is Proteasome-dependent and Does Not Require Lys-8—The demonstrated degradation of two forms of the wild-type rat ^{MLS}rAANAT$_{3f}$ (Ac-^{MLS}rAANAT$_{3f}$ and its non-Nt-acetylated counterpart) by the two branches of the N-end rule pathway (Fig. 2) already implied the proteasome dependence of this degradation, given the known organization of the N-end rule pathway (Fig. 1, *A* and *B*). To verify this in *S. cerevisiae* by independent means, CHX-chases with rat ^{MLS}rAANAT$_{3f}$ were carried out in wild-type *versus pdr5*Δ cells in either the presence or absence of the MG132 proteasome inhibitor. (Cells lacking the transmembrane transporter PDR5 are more sensitive to MG132 (77, 78).)

As expected, given the proteasome dependence of the N-end rule pathway (Fig. 1, *A* and *B*), the normally rapid degradation of the wild-type rat ^{MLS}rAANAT$_{3f}$ was substantially inhibited in wild-type *S. cerevisiae* in the presence of 50 μM MG132 (Fig. 4, *A* and *B*). This degradation was inhibited even more strongly in mutant *pdr5*Δ cells under the same conditions, confirming the proteasome dependence of at least the bulk of ^{MLS}rAANAT$_{3f}$ degradation (Fig. 4, *A* and *B*).

N-terminal regions of mammalian AANATs contain a highly conserved Lys residue (*e.g.* Lys-8 in rat AANAT and Lys-10 in human AANAT) that has been suggested as a potential ubiquitylation site and thus a determinant of the AANAT degron (33, 79–81). To address this possibility, CHX-chases were performed in *S. cerevisiae* with wild-type ^{MLS}rAANAT$_{3ha}$ and a mutant containing a Lys-8 → Arg mutation (^{MLS}rAANAT$^{K8R}_{3ha}$). Wild-type ^{MLS}rAANAT$_{3ha}$ and the mutant ^{MLS}rAANAT$^{K8R}_{3ha}$ were degraded at similar rates, indicating that the conserved lysine at this position (Lys-8 in rat ^{MLS}rAANAT) is not, by itself, a significant determinant of ^{MLS}rAANAT stability (Fig. 4*C*).

Degradation of Human AANAT in S. cerevisiae—Fig. 3 (*A* (*lanes 6–9*) and *B*) shows the results of a CHX-chase, in wild-type yeast, with the 207-position residue (not counting the tag) $^{(M)ST}$hAANAT$_{3f}$, the wild-type human AANAT C-terminally tagged with a triple-FLAG epitope. Parentheses around the superscript's N-terminal Met residue denote the fact that this Met is cotranslationally cleaved off by MetAPs. Whereas human $^{(M)ST}$hAANAT$_{3f}$ was relatively unstable in *S. cerevisiae* ($t_{1/2} \approx 30$ min), it was much longer-lived (including its higher zero-time, prechase level) than the wild-type rat ^{MLS}rAANAT$_{3f}$ under the same conditions (Fig. 3, *A* and *B*).

As was also done with the wild-type rat ^{MLS}rAANAT$_{3f}$ (Fig. 2*C*), we characterized the degradation of wild-type human $^{(M)ST}$hAANAT$_{3f}$ in *S. cerevisiae* strains deficient in specific components of the N-end rule pathway. The N-terminal Ser-Thr sequence of wild-type human $^{(M)ST}$hAANAT$_{3f}$ (after the cotranslational removal of the initially present N-terminal Met) made it likely that $^{(M)ST}$hAANAT$_{3f}$ was cotranslationally Nt-acetylated *in vivo* (59, 63). This modification of human $^{(M)ST}$hAANAT$_{3f}$ would make it a potential target for degradation by the Ac/N-end rule pathway (Fig. 1*B*). In contrast, the non-Nt-acetylated human $^{(M)ST}$hAANAT$_{3f}$ would not be expected to be recognized by either the Ac/N-end rule or the Arg/N-end rule pathway (Fig. 1*A*), in the latter case due to the absence of both a destabilizing N-terminal residue and a bulky hydrophobic (Φ) second residue. (A Met-Φ N-terminal motif, containing a second-position Φ residue, can act as an N-degron recognized by the Arg/N-end rule pathway (60, 82).

Indeed, the rate of degradation of human $^{(M)ST}$hAANAT$_{3f}$ in *ubr1*Δ *S. cerevisiae*, which lacked the Ubr1 N-recognin and therefore lacked the Arg/N-end rule pathway (Fig. 1*A*), was similar to the rate of $^{(M)ST}$hAANAT$_{3f}$ degradation in wild-type cells (Fig. 3, *C* (*lanes 1–4 versus lanes 9–12*), *D* (*lanes 2–5 versus lanes 14–17*), *E*, and *F*). The rate of $^{(M)ST}$hAANAT$_{3f}$ degradation that was observed with wild-type *S. cerevisiae* was also not significantly changed in *doa10*Δ cells, which lacked one of two known Ac/N-recognins of the Ac/N-end rule pathway (Figs. 1*B* and 3, *D* (*lanes 10–13 versus lanes 2–5*) and *F*). Surprisingly, however, $^{(M)ST}$hAANAT$_{3f}$ was strongly destabilized in *naa10*Δ cells, which lacked the cognate Nt-acetylase for the N-terminal Ser residue (59, 62); similar results were obtained with double-mutant *naa10*Δ *ubr1*Δ cells (Fig. 3, *C–F*).

Given the much faster degradation of $^{(M)ST}$hAANAT$_{3f}$ in the absence of Naa10 (*e.g.* Fig. 3, *C* (*lanes 1–4 versus lanes 5–8*) and *E*) (*i.e.* in cells that would be incapable of Nt-acetylating $^{(M)ST}$hAANAT$_{3f}$), we also carried out CHX-chases, in wild-type *S. cerevisiae*, with $^{(M)PT}$hAANAT$_{3f}$. In the latter mutant, the N-terminal Ser was replaced by the non-Nt-acetylatable Pro residue. In contrast to wild-type $^{(M)ST}$hAANAT$_{3f}$ in *naa10*Δ cells, in which the (non-Nt-acetylated) $^{(M)ST}$hAANAT became strikingly short-lived, the (non-Nt-acetylatable) $^{(M)PT}$hAANAT mutant was found to be longer-lived, in wild-type cells, than the Nt-acetylatable wild-type $^{(M)ST}$hAANAT$_{3f}$ (Fig. 4, *D* and *E*). These results indicated that the observed accelerated degradation of the wild-type human

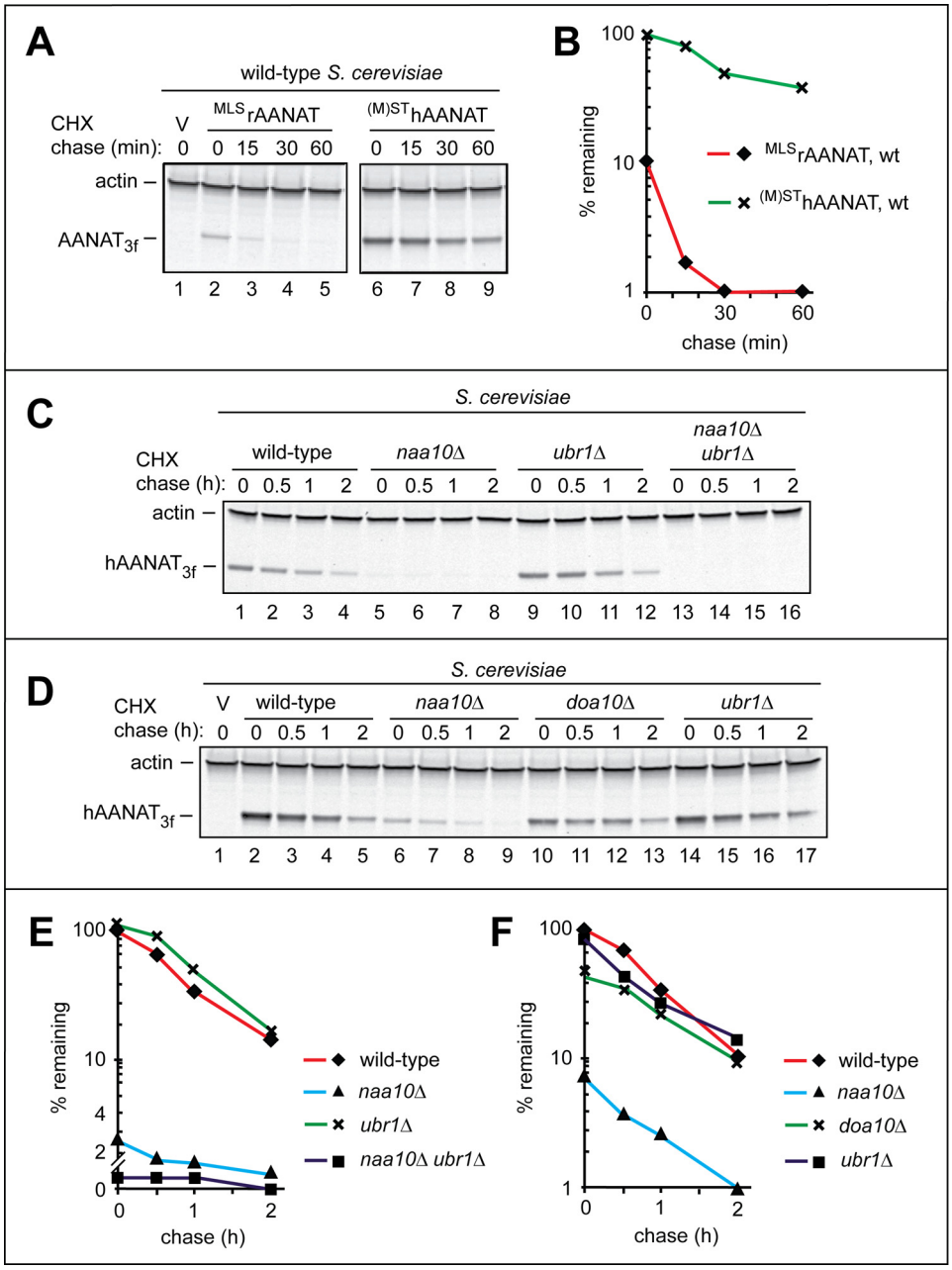

FIGURE 3. **Degradation assays with the wild-type human $^{(M)ST}$hAANAT in *S. cerevisiae*.** *A*, comparison of degradation rates of the wild-type rat ^{MLS}rAANAT$_{3f}$ and the wild-type human $^{(M)ST}$hAANAT$_{3f}$ in *S. cerevisiae*. Immunoblotting with antibody to actin was used as a loading control. *Lane 1*, wild-type *S. cerevisiae* were transformed with vector (*V*) alone (control). CHX-chases were performed at 30 °C for the indicated times in wild-type *S. cerevisiae* with the wild-type rat ^{MLS}rAANAT$_{3f}$ (*lanes 2–5*) and with the wild-type human $^{(M)ST}$hAANAT$_{3f}$ (*lanes 6–9*). The bands of AANAT and actin are indicated on the *left*. *B*, quantification of data in *A*. *C*, CHX-chases with the wild-type human $^{(M)ST}$hAANAT$_{3f}$ in wild-type *S. cerevisiae* (*lanes 1–4*) and its mutants *naa10*Δ (*lanes 5–8*), *ubr1*Δ (*lanes 9–12*), and *naa10*Δ *ubr1*Δ (*lanes 13–16*). The bands of human $^{(M)ST}$hAANAT$_{3f}$ and actin are indicated on the *left*. *D*, *lane 1*, wild-type *S. cerevisiae* were transformed with vector (*V*) alone (control). Shown are CHX-chases with the wild-type human $^{(M)ST}$hAANAT$_{3f}$ in wild-type *S. cerevisiae* (*lanes 2–5*) and its mutants *naa10*Δ (lanes 6–9), *doa10*Δ (*lanes 10–13*), and *ubr1*Δ (*lanes 14–17*). The bands of human $^{(M)ST}$hAANAT$_{3f}$ and actin are indicated on the *left*. *E*, quantification of data in *C*. *F*, quantification of data in *D*. All quantified CHX-chase assays were carried out at least three times and yielded results within 10% of the data shown.

$^{(M)ST}$hAANAT in *naa10*Δ *S. cerevisiae* was not caused by the failure to Nt-acetylate $^{(M)ST}$hAANAT in the absence of the NatA Nt-acetylase.

We do not understand the mechanistic cause of the (reproducibly observed) much faster degradation of human $^{(M)ST}$hAANAT in *naa10*Δ *S. cerevisiae* (Fig. 3, *C–F*). One possibility, which remains to be examined, is the apparent inhibition of the yeast Hsp90 chaperone system (centered on the *S. cerevisiae* Hsc82/Hsp82 proteins) in *naa10*Δ cells.[3] If human $^{(M)ST}$hAANAT expressed in wild-type *S. cerevisiae* is a protected (from degradation) client of the Hsc82/Hsp82 system, a failure of this protection in *naa10*Δ mutant cells would make $^{(M)ST}$hAANAT vulnerable to a currently unknown pathway of

[3] J.-H. Oh and A. Varshavsky, unpublished data.

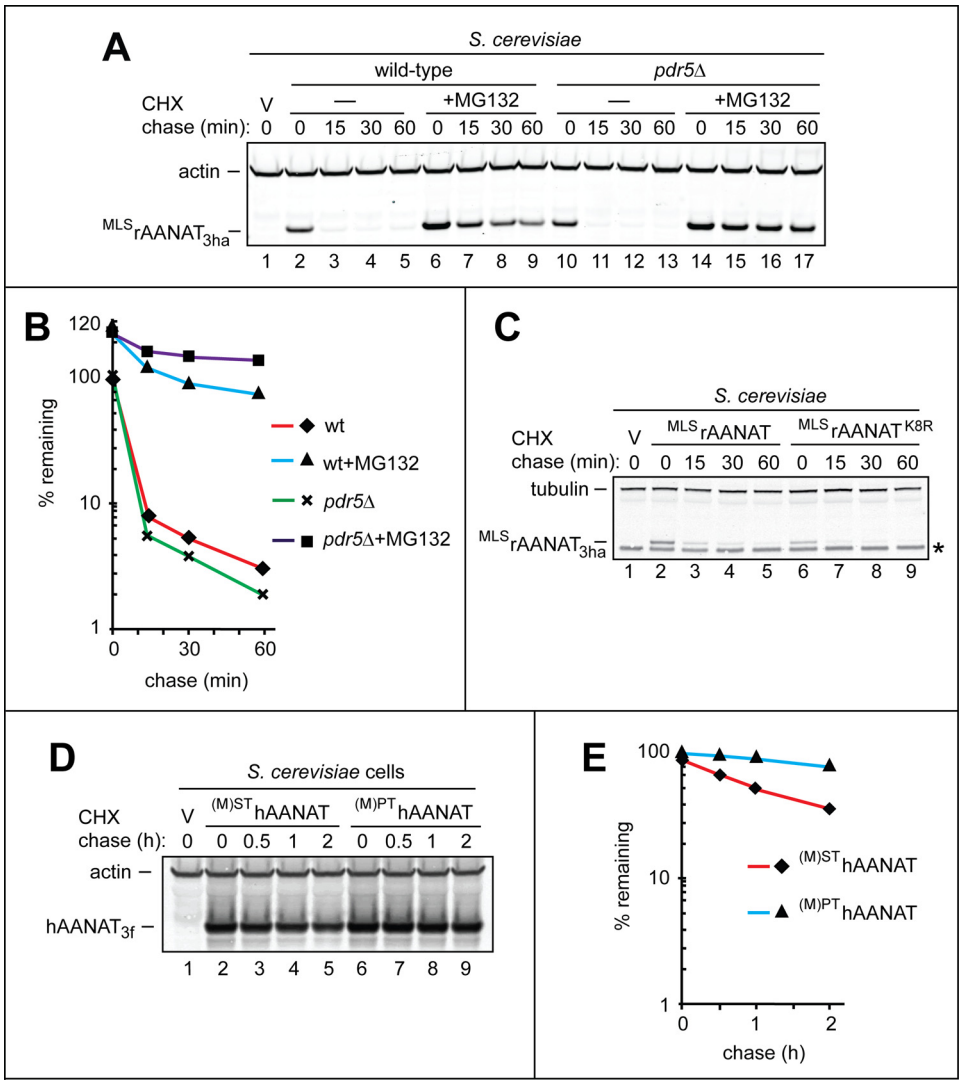

FIGURE 4. **Degradation assays with a proteasome inhibitor and AANAT mutants in *S. cerevisiae*.** *A*, *lane 1*, wild-type *S. cerevisiae* were transformed with vector (*V*) alone (control). *Lanes 2–5*, CHX-chase was performed at 30 °C for the indicated times in wild-type *S. cerevisiae* with the wild-type rat ^{MLS}rAANAT$_{3ha}$. *Lanes 6–9*, same as in *lanes 2–5*, but the CHX-chase was in the presence of the MG132 proteasome inhibitor (see "Experimental Procedures"). *Lanes 10–13*, same as in *lanes 2–5* but in *pdr5*Δ *S. cerevisiae* lacking the efflux pump Pdr5. *Lanes 14–17*, same as in *lanes 10–13* but in the presence of MG132. The bands of actin and ^{MLS}rAANAT$_{3ha}$ are indicated on the *left*. *B*, quantification of data in *A*. *C*, CHX-chases were performed in wild-type *S. cerevisiae* with the wild-type rat ^{MLS}rAANAT$_{3ha}$ (*lanes 2–5*) and with its Lys-8 → Arg mutant ^{MLS}rAANAT$^{K8R}_{3ha}$ (see "Results"). The bands of tubulin and AANAT are indicated on the left. An *asterisk* on the *right* denotes a band of protein that cross-reacted with anti-HA antibody (the band is also present in *lane 1*, the vector-only control). *D*, *lane 1*, wild-type *S. cerevisiae* were transformed with vector (*V*) alone (control). *Lanes 2–5*, CHX-chase was performed at 30 °C for the indicated times in wild-type *S. cerevisiae* with the wild-type human $^{(M)ST}$hAANAT$_{3f}$. *Lanes 6–9*, same as in *lanes 2–5* but with the mutant human $^{(M)PT}$hAANAT$_{3f}$. The bands of actin and AANAT are indicated on the *left*. *E*, quantification of data in *A*. All quantified CHX-chase assays were carried out at least three times and yielded results within 10% of the data shown.

the Ub system that is distinct from the Arg/N-end rule pathway. (A proteolytic pathway in question would be distinct from the Arg/N-end rule pathway because $^{(M)ST}$hAANAT was equally short-lived in single-mutant *naa10*Δ and double-mutant *naa10*Δ *ubr1*Δ cells (Fig. 3, *C–F*).) In sum, the above Hsp90-based mechanism (which remains to be addressed in the context of the $^{(M)ST}$hAANAT protein) might underlie the strongly accelerated degradation of $^{(M)ST}$hAANAT in *naa10*Δ *S. cerevisiae*.

Degradation of Rat AANAT in Human HEK293T Cells—To compare the relative rates of degradation of N-terminal mutants of rat AANAT in human HEK293T cells, the wild-type rat ^{MLS}rAANAT$_{3f}$ and its mutants $^{(M)SMLS}$rAANAT$_{3f}$, $^{(M)SI}$rAANAT$_{3f}$, and $^{(M)PLS}$rAANAT$_{3f}$ (see items i–iv at the beginning of "Results") were expressed in these cells using transient transfection. Preliminary experiments with wild-type ^{MLS}rAANAT$_{3f}$ encoded by a pcDNA3-based plasmid and expressed from the full-strength P_{CMV} promoter indicated that the levels of expression of ^{MLS}rAANAT$_{3f}$ were high enough to saturate or nearly saturate pathways that targeted ^{MLS}rAANAT$_{3f}$ for degradation in HEK293T cells. Specifically, at those (high) levels of expression, wild-type rat ^{MLS}rAANAT$_{3f}$ either was stable or was degraded slowly (data not shown).

We addressed this problem by constructing a set of truncated derivatives of the original P_{CMV} promoter, aiming to attenuate its activity. The resulting nested set of truncated promoters, denoted as P_{CMVt1}, P_{CMVt2}, and P_{CMVt3}, comprised progressively shortened versions of the original P_{CMV}. These truncations (Fig. 5*A*) were similar (although not identical) to a series of P_{CMV} truncations described earlier by

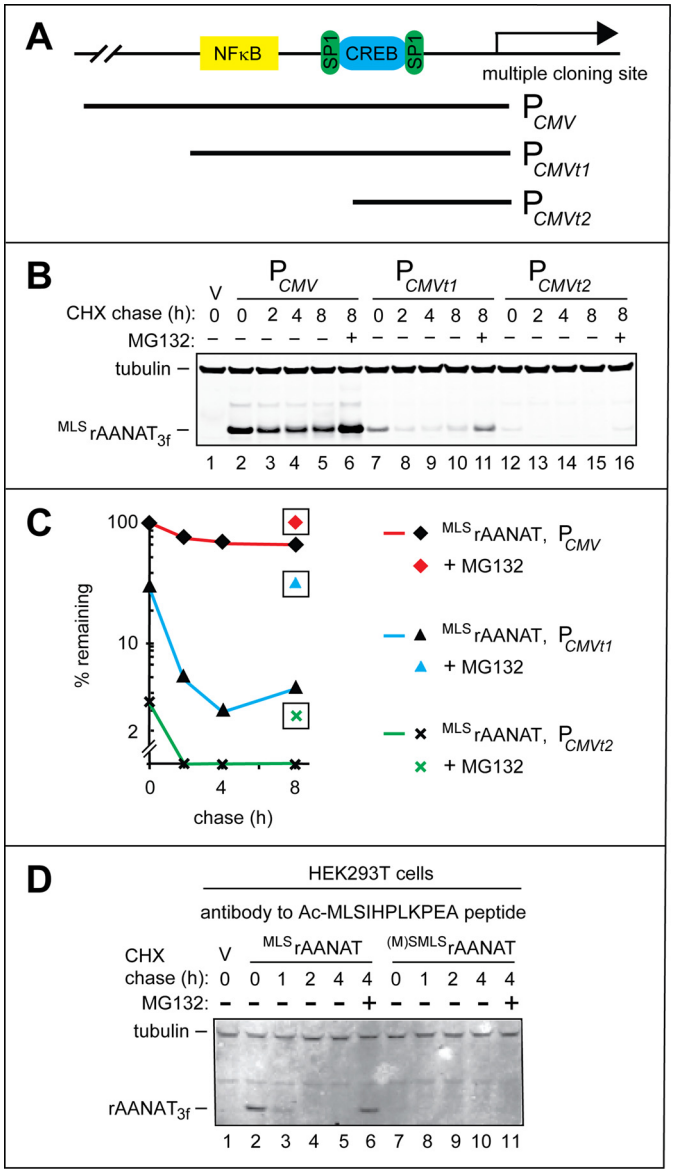

FIGURE 5. **Weakened derivatives of the PCMV promoter in HEK293T cells and degradation assays using antibody to Nt-acetylated rat ^{MLS}rAANAT.** *A*, a simplified diagram of the "wild-type" (unmodified) P_{CMV} promoter in the cloning vector, with schematically illustrated binding sites for the NFκB, SP1, and CREB transcriptional regulators. Two 5′-terminal truncations of wild-type P_{CMV}, denoted as P_{CMVt1} and P_{CMVt2}, are also indicated. *B*, *lane 1*, HEK293T cells were transformed with vector (*V*) alone (control). CHX-chases were performed at 37 °C for the indicated times in HEK293T cells with the wild-type rat ^{MLS}rAANAT$_{3f}$ expressed either from the unmodified P_{CMV} promoter (*lanes 2–5*), from the P_{CMVt1} promoter (*lanes 7–10*), or from the P_{CMVt2} promoter (*lanes 12–15*). *Lanes 6*, *10*, and *16*, same as *lanes 5*, *9*, and *15* except that the MG132 proteasome inhibitor was present during 8-h CHX-chases in each case (see "Experimental Procedures" and "Results"). The bands of tubulin and ^{MLS}rAANAT$_{3f}$ are indicated on the *left*. *C*, quantification of data in *B*. *Symbols shown separately* and *framed* in *black squares* correspond to altered (increased) levels of test proteins in the presence of MG132. All quantified CHX-chase assays were carried out at least three times and yielded results within 10% of the data shown. *D*, immunoblotting with affinity-purified antibody to Nt-acetylated ^{MLS}rAANAT (see "Experimental Procedures"). *Lane 1*, HEK293T cells were transformed with vector (*V*) alone (control) bearing the (weakened) P_{CMVt1} promoter. CHX-chases were performed at 30 °C for the indicated times in HEK293T cells with the wild-type rat ^{MLS}rAANAT$_{3f}$ (*lanes 2–5*) and its mutant $^{(M)SMLS}$rAANAT$_{3f}$ (*lanes 7–10*). *Lanes 6* and *11*, same as *lanes 5* and *10* except that the MG132 proteasome inhibitor was present during 4-h CHX-chases in each case (see "Experimental Procedures"). The bands of rAANAT and tubulin (the latter a loading control) are indicated on the *left*.

Promega Inc. (83). Each of the P_{CMVt1}, P_{CMVt2}, and P_{CMVt3} promoter variants was cloned into pcDNA3, replacing full-length P_{CMV}.

The wild-type rat ^{MLS}rAANAT$_{3f}$ was cloned into each of the above pcDNA3-based plasmids, and CHX-chases were performed in HEK293T cells transiently transfected with these constructs. Expression of ^{MLS}rAANAT$_{3f}$ from the P_{CMVt1} and P_{CMVt2} promoters reduced time-zero levels of ^{MLS}rAANAT$_{3f}$ (measured by immunoblotting at the beginning of CHX-chase) by ~70% and by ~97%, respectively, in comparison with the unmodified P_{CMV} promoter (Fig. 5, *A–C*). With the most truncated promoter, P_{CMVt3}, no ^{MLS}rAANAT$_{3f}$ could be detected at the same level of immunoblotting sensitivity (data not shown). The lower levels of ^{MLS}rAANAT$_{3f}$ expression that have been attained through the use of the P_{CMVt1} and P_{CMVt2} promoters resulted in a strongly increased rate of the post-translational degradation of ^{MLS}rAANAT$_{3f}$ ($t_{½} < 2$ h *versus* $t_{½} > 8$ h when ^{MLS}rAANAT$_{3f}$ was expressed from the full-length P_{CMV} promoter; Fig. 5, *A–C*). Treatment of HEK293T cells with the proteasome inhibitor MG132 during the chase increased the levels of ^{MLS}rAANAT$_{3f}$ expressed from these promoters, thereby confirming that in each case, the bulk of degradation was proteasome-dependent (Fig. 5, *A–C*). The pcDNA3$_{CMVt1}$ plasmid, which contained P_{CMVt1}, one weakened version of the P_{CMV} promoter, was chosen for experiments with HEK293T cells in this study.

In agreement with the relative metabolic stabilities of AANAT proteins expressed in *S. cerevisiae* (Fig. 1, *A* and *B*), the mutant rat $^{(M)SI}$rAANAT$_{3f}$, bearing a deletion of the Leu residue at position 2 of wild-type ^{MLS}rAANAT$_{3f}$ (Fig. 2*A*), was the longest-lived protein in the set of rat AANAT mutants examined in HEK293T cells ($t_{½} > 4$ h; Fig. 6, *A* (*lanes 12–16*) and *C*). The wild-type rat ^{MLS}rAANAT$_{3f}$ and its $^{(M)SMLS}$rAANAT$_{3f}$ mutant (see items i and ii at the beginning of "Results") were significantly shorter-lived in HEK293T cells than $^{(M)SI}$rAANAT$_{3f}$, with $t_{½} \approx 1$ h and $t_{½} < 1$ h, respectively, *versus* $t_{½} > 4$ h (Fig. 6, *A* (*lanes 2–11*) and *C*).

We expected, *a priori*, that $^{(M)SMLS}$rAANAT$_{3f}$ would initiate from the first encoded Met residue, particularly because of the inclusion of the Kozak "optimal" upstream sequence in the relevant plasmids used for expression of test AANAT proteins. We could verify that expectation through chase-degradation assays using an affinity-purified antibody against the Nt-acetylated N terminus of ^{MLS}rAANAT$_{3f}$ (Fig. 5*D*). We produced and purified this antibody as described under "Experimental Procedures." As shown in Fig. 5*D*, immunoblotting of SDS-PAGE-fractionated samples containing ^{MLS}rAANAT$_{3f}$ or $^{(M)SMLS}$rAANAT$_{3f}$ with the anti-Ac- ^{MLS}rAANAT antibody generated a positive signal only in samples expressing ^{MLS}rAANAT$_{3f}$. If a construct expressing $^{(M)SMLS}$rAANAT$_{3f}$ had initiated translation (to a significant extent) from the second Met residue, the resulting translated protein would have been ^{MLS}rAANAT$_{3f}$. However, no signal was detected (using the above anti-Ac-^{MLS}rAANAT antibody) with samples containing $^{(M)SMLS}$rAANAT$_{3f}$ (Fig. 5*D*), indicating negligible levels of translation initiation at the position 2 Met.

Although the mutant $^{(M)PLS}$rAANAT$_{3f}$ was partially stabilized relative to wild-type ^{MLS}rAANAT$_{3f}$, the former protein

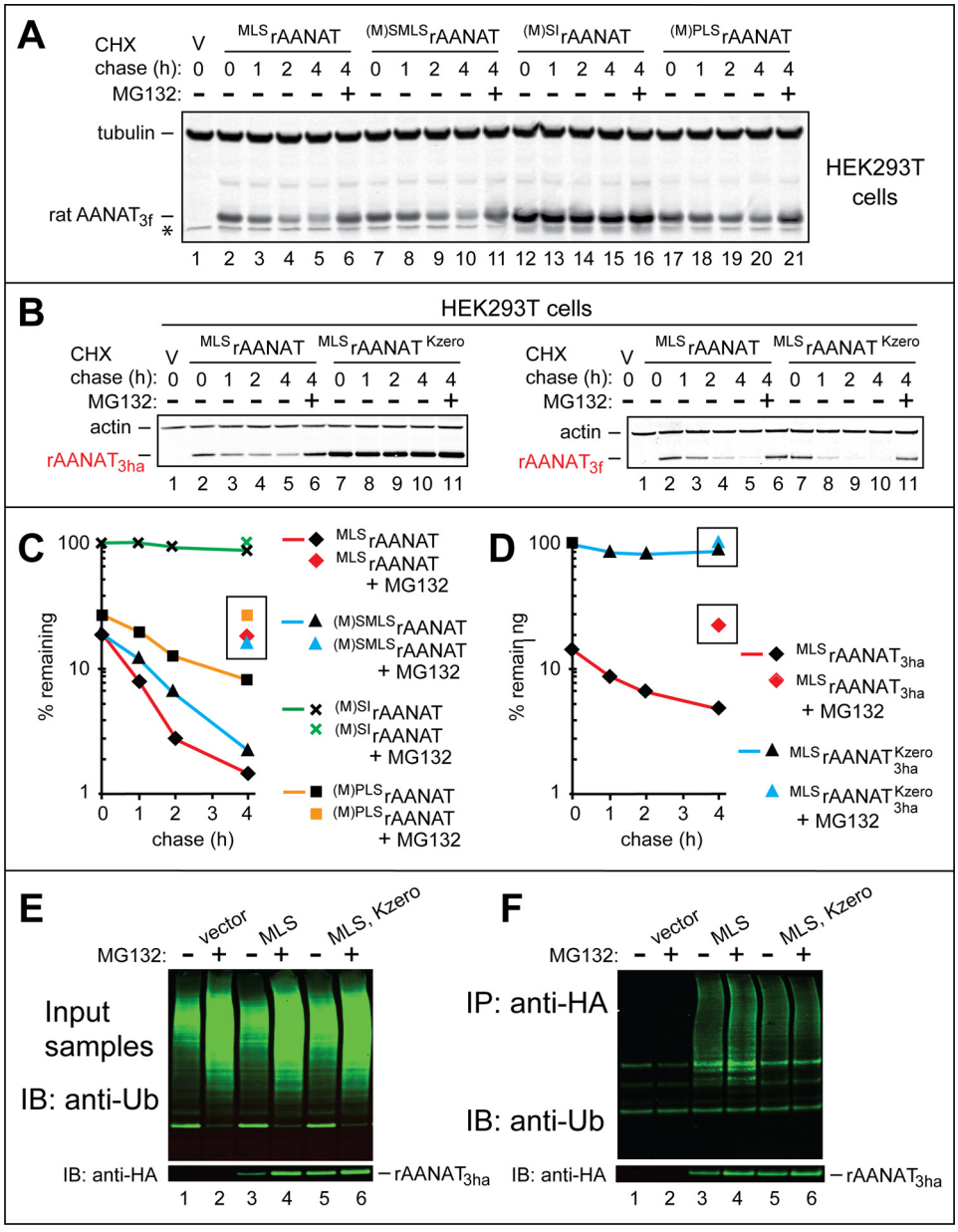

FIGURE 6. **Degradation and ubiquitylation assays with rat and human AANATs in human HEK293T cells.** *A*, *lane 1*, HEK293T cells were transformed with vector (*V*) alone (control) bearing the (weakened) P_{CMVt1} promoter (see "Results" and Fig. 5, *A–C*). Immunoblotting with antibody to tubulin was used as a loading control. CHX-chases were performed at 37 °C for the indicated times in HEK293T cells with the wild-type rat ^{MLS}rAANAT$_{3f}$ (*lanes 2–5*) and with its mutants $^{(M)SMLS}$rAANAT$_{3f}$ (*lanes 7–10*), $^{(M)SI}$rAANAT$_{3f}$ (*lanes 12–15*), and $^{(M)PLS}$rAANAT$_{3f}$ (*lanes 17–20*). *Lanes 6*, *11*, *16*, and *21*, same as *lanes 5*, *10*, *15*, and *20* except that the MG132 proteasome inhibitor was present during a 4-h CHX-chase in each case (see "Experimental Procedures"). The bands of AANAT$_{3f}$ and tubulin are indicated on the *right*. An *asterisk* on the *left* denotes a band of protein that cross-reacted with anti-FLAG antibody (the band is also present in *lane 1*, the vector-only control). *B*, *left*, *lane 1*, same as the control in *lane 1* of *A*. CHX-chases were performed at 37 °C for the indicated times in HEK293T cells with the wild-type rat ^{MLS}rAANAT$_{3ha}$ (*lanes 2–5*) and with its lysine-lacking mutant ^{MLS}rAANAT$^{Kzero}_{3ha}$ (*lanes 7–10*). *Lanes 6* and *11*, same as *lanes 5* and *10* except that MG132 was present during a 4-h CHX-chase in each case. *Right*, same as in the *left panel*, but both the wild-type ^{MLS}rAANAT$_{3f}$ and its lysine-lacking counterpart were C-terminally tagged with a triple-FLAG tag, which contains a Lys residue, in contrast to the HA tag, which lacks lysines (see "Results" and "Discussion"). *C*, quantification of data in *A*. *D*, quantification of data in *B*. *Symbols shown separately* and *framed* in *black squares* or *rectangles* correspond to altered levels of test proteins in the presence of MG132. All quantified CHX-chase assays were carried out at least three times and yielded results within 10% of the data shown. *E*, immunoblot analyses (*IB*), using anti-Ub antibody, of total, input (before immunoprecipitation) extracts from HEK293T cells that had been transfected either with vector alone (*lanes 1* and *2*) or with plasmid expressing the wild-type rat ^{MLS}rAANAT$_{3ha}$ (*lanes 3* and *4*) or with plasmid expressing its lysine-lacking counterpart ^{MLS}rAANAT$^{Kzero}_{3ha}$ (*lanes 5* and *6*). The MG132 proteasome inhibitor was either omitted (*lanes 1*, *3*, and *5*) or added to HEK293T cells (to a final concentration of 10 μM) 6 h before preparation of extracts (*lanes 2*, *4*, and *6*). The *bottom panel* shows the results of detecting non-ubiquitylated ^{MLS}rAANAT$_{3ha}$ (absent in the *control lanes 1* and *2*) with anti-HA antibody. *F*, same as in *E* but immunoblot analyses (using anti-Ub antibody) of the input samples after their immunoprecipitation (*IP*) with anti-HA antibody (followed by SDS-PAGE) to isolate and detect ubiquitylated AANAT$_{3ha}$ species.

was still significantly shorter-lived ($t_{½} \approx 2$ h) than the most stable $^{(M)SI}$rAANAT$_{3f}$ mutant (Fig. 6, *A* (*lanes 17–21*) and *C*). Although N-terminal Pro is not Nt-acetylated (59, 63) (this makes N-terminal Pro-bearing proteins invulnerable to the Ac/N-end rule pathway), the N-terminal Pro residue might still be (weakly) recognized by the Arg/N-end rule pathway in some sequence contexts. Specifically, our SPOT-type, peptide-based binding assays (84) suggested that the Ubr1 N-recognin of the

S. cerevisiae Arg/N-end rule pathway (and, by inference, mammalian Ubr1 and Ubr2 as well) may weakly bind to N-terminal Pro when this residue is followed by a hydrophobic residue.[4] Thus, one interpretation of the "residual" instability of the rat $^{(M)PLS}$rAANAT$_{3f}$ mutant (in comparison with the longest-lived $^{(M)SI}$rAANAT$_{3f}$ mutant) is that the (non-Nt-acetylated) N-terminal sequence Pro-Leu of $^{(M)PLS}$rAANAT$_{3f}$ is weakly targeted by the Arg/N-end rule pathway, in contrast to the absence of targeting of the N-terminal Ser-Ile sequence of the $^{(M)SI}$rAANAT$_{3f}$ mutant (Fig. 6, *A* and *C*; also see Fig. 2, *B* and *D*).

As mentioned above, we found that transient transfection-based expression of AANAT from the full-strength P_{CMV} promoter could be high enough to result in saturation or near saturation of the relevant proteolytic pathways. Although the use of the considerably weaker P_{CMVt1} promoter at least partially solved this problem (see above), additional studies would be required to make sure that pathway saturation effects were consistently negligible with longer-lived AANAT derivatives that were expressed from P_{CMVt1}. That said, the preponderance of our data makes it nearly certain that the observed differences in time-zero (before chase) levels of AANAT proteins were caused largely by differences in the rates of their degradation.

The Bulk of Degradation of Rat AANAT Is Mediated by Polyubiquitylation of Its Lys Residue(s)—An earlier study, in which the wild-type rat ^{MLS}rAANAT was apparently not stabilized by conversion of its Lys residues to Arg, was based on measurements of steady-state levels of ^{MLS}rAANAT in HEK293 cells that had been treated or left untreated with the proteasome inhibitor MG132 (37). To address this issue more directly, we generated a triple-HA-tagged mutant, denoted ^{MLS}rAANAT$^{Kzero}_{3ha}$, of the wild-type rat ^{MLS}rAANAT in which all four of its Lys residues were converted to Arg. (A FLAG-based epitope tag could not be employed in these experiments, because FLAG contains a Lys residue that could potentially serve as a target for polyubiquitylation.)

CHX-chases in HEK293T cells (performed as described above) with the wild-type ^{MLS}rAANAT$_{3ha}$ *versus* its lysine-lacking ^{MLS}rAANAT$^{Kzero}_{3ha}$ mutant indicated that ^{MLS}rAANAT$^{Kzero}_{3ha}$ was nearly completely stable during the chase ($t_{½} \gg 4$ h), whereas the wild-type ^{MLS}rAANAT$_{3ha}$ was degraded, with $t_{½} \approx 2$ h (Fig. 6, *B* and *D*). A treatment with MG132 during CHX-chase strongly stabilized the wild-type ^{MLS}rAANAT$_{3ha}$, confirming that its degradation is proteasome-dependent (Fig. 6, *B* (*left*, *lanes 2* and *6*) and *D*). In contrast, the MG132 treatment during CHX-chase of the lysine-lacking ^{MLS}rAANAT$^{Kzero}_{3ha}$ mutant produced at most a marginal stabilizing effect, suggesting that even if there is a small (residual) amount of lysine-independent degradation of ^{MLS}rAANAT$^{Kzero}_{3ha}$, such a degradation would still require the proteasome (Fig. 6, *B* (*left*, *lanes 7* and *11*) and *D*).

In a different approach to the same problem, HEK293T cells were transiently transfected with the pcDNA3 vector or with plasmids expressing either ^{MLS}rAANAT$_{3ha}$ or ^{MLS}rAANAT$^{Kzero}_{3ha}$. Cells were then treated for 6 h with either MG132 or an equivalent volume of DMSO (in which the stock solution of MG132 was made). Thereafter, cell extracts were immunoprecipitated with anti-HA magnetic beads, and the immunoprecipitates were fractionated by SDS-PAGE, followed by immunoblotting with anti-HA and anti-ubiquitin antibodies. Polyubiquitin chains (apparently linked to ^{MLS}rAANAT$_{3ha}$) could be readily detected in fractionated immunoprecipitates of extracts from cells that expressed ^{MLS}rAANAT$_{3ha}$ (but, crucially, not from cells that expressed an empty vector), and the levels of polyubiquitin chains were significantly increased in the presence of MG132 (Fig. 6*F*, *lanes 1–4*). In contrast, significantly lower amounts of polyubiquitin chains were observed in fractionated immunoprecipitates of extracts from cells that expressed the lysine-lacking ^{MLS}rAANAT$^{Kzero}_{3ha}$ (Fig. 6*F*, *lane 5*). Moreover, the presence of MG132 did not increase the low levels of detected polyubiquitin chains (Fig. 6*F*, *lane 5 versus lane 6*). The latter result suggested that (residual) polyubiquitin chains observed in cells that expressed ^{MLS}rAANAT$^{Kzero}_{3ha}$ may be of a kind (*e.g.* see Ref. 85) that do not contribute to the proteasome-dependent degradation of ^{MLS}rAANAT$^{Kzero}_{3ha}$. In agreement with this interpretation, the lysine-lacking ^{MLS}rAANAT$^{Kzero}_{3ha}$ mutant was expressed at significantly higher steady-state levels than the wild-type rat ^{MLS}rAANAT$_{3ha}$ in the absence of MG132 (in DMSO-treated cells) (Fig. 6*E*, *bottom*), suggesting that the absence of Lys residues stabilized ^{MLS}rAANAT$^{Kzero}_{3ha}$ against degradation throughout life histories of ^{MLS}rAANAT$^{Kzero}_{3ha}$ molecules, including, possibly, their degradation during or immediately after their synthesis.

Degradation of Human AANAT in Human HEK293T Cells—Degradation of the wild-type human $^{(M)ST}$hAANAT$_{3f}$ and its N-terminal Pro residue-bearing mutant $^{(M)PT}$hAANAT$_{3f}$ (see items vi and vii at the beginning of "Results") were examined by CHX-chases in HEK293T cells. In agreement with the findings in *S. cerevisiae* (Figs. 2 and 3), the wild-type human $^{(M)ST}$hAANAT was longer-lived than the wild-type rat ^{MLS}rAANAT$_{3f}$ in HEK293T cells (compare Fig. 7*A* with Fig. 6*A*). Interestingly, the mutant human $^{(M)PT}$hAANAT$_{3f}$ was less stable than the wild-type human ^{MLS}rAANAT$_{3f}$ during the course of a 2-h chase in HEK293T cells (Fig. 7, *A* and *C*).

We also asked whether the (relatively slow) degradation of the wild-type human $^{(M)ST}$hAANAT$_{3f}$ (Fig. 7, *A* and *C*) required both its lysine-dependent ubiquitylation and the proteasome. CHX-chases were carried out with $^{(M)ST}$hAANAT$_{3ha}$ and its lysine-lacking mutant $^{(M)ST}$hAANAT$^{Kzero}_{3ha}$. The latter protein was stable during the chase ($t_{½} \gg 4$ h), whereas wild-type $^{(M)ST}$hAANAT$_{3ha}$ exhibited a weak but observable instability (Fig. 7, *B* and *D*). Treatment with the MG132 proteasome inhibitor increased the level of the wild-type human $^{(M)ST}$hAANAT$_{3ha}$ during CHX-chase, confirming proteasome dependence of its (slow) degradation (Fig. 7, *B* (*lanes 3* and *7*) and *D*).

Discussion

The ~23-kDa AANAT (also called serotonin *N*-acetyltransferase) is apparently universal among animals and is present in plants as well. AANAT converts the neurotransmitter serotonin to NAS, a regulatory compound in its own right and the immediate precursor of melatonin, a circulating hormone that regulates sleep and other circadian processes in vertebrates. The levels of melatonin and NAS are modulated by oscillatory circadian circuits and also impact those circuits, in addition to

[4] J.-H. Oh, B. Wadas, and A. Varshavsky, unpublished data.

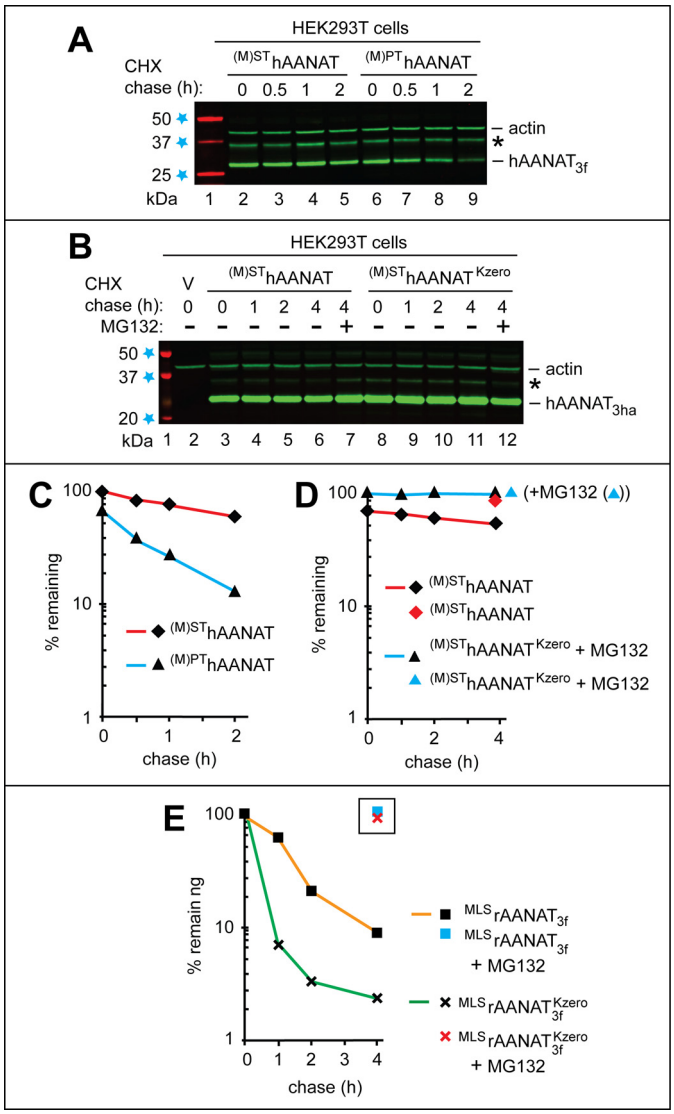

FIGURE 7. **Degradation of the wild-type human $^{(M)ST}$hAANAT and its mutants in human HEK293T cells.** The test proteins were expressed in HEK293T cells using a plasmid bearing the (weakened) P_{CMVt1} promoter (see "Results" and see Fig. 5, *A–C*). *A*, *lane 1*, fluorescently labeled molecular mass markers (LI-COR), with their masses, in kDa, indicated on the *left*. CHX-chases were performed at 37 °C for the indicated times in HEK293T cells with the wild-type human $^{(M)ST}$hAANAT$_{3f}$ (*lanes 2–5*) and with its mutant $^{(M)PT}$hAANAT$_{3f}$ (*lanes 6–9*). *B*, *lane 1*, fluorescently labeled molecular mass markers, with their masses, in kDa, indicated on the *left*. *Lane 2*, HEK293T cells were transformed with vector (*V*) alone (control). CHX-chases were performed at 37 °C for the indicated times in HEK293T cells with the wild-type human $^{(M)ST}$hAANAT$_{3ha}$ (*lanes 3–6*) and with its lysine-lacking mutant $^{(M)ST}$hAANAT$^{Kzero}_{3ha}$ (*lanes 8–11*). *Lanes 7* and *12*, same as *lanes 6* and *11*, except that the MG132 proteasome inhibitor was present during a 4-h CHX-chase in each case (see "Experimental Procedures"). The bands of actin and AANAT are indicated on the *right*. *Asterisks* on the *right* in *A* and *B* denote a protein band (possibly the same protein and possibly a derivative of AANAT) that reacted with both anti-FLAG antibody in *A* and anti-HA antibody in *B*. *C*, quantification of data in *A*. *D*, quantification of data in *B*. *E*, quantification of data in Fig. 6*B* (*right*), similar to the analogous quantifications described in the legend to Fig. 6, *C* and *D*. All quantified CHX-chase assays were carried out at least three times and yielded results within 10% of the data shown.

other effects of these compounds (see the Introduction). Hence the importance of temporal control of the AANAT enzyme. The expression of AANAT is regulated through both transcriptional and post-translational mechanisms. Details of these mechanisms differ among vertebrates. In addition, although AANAT enzymes from different species are highly sequelogous (71) throughout their ORFs, the sequences of the first ~10 residues of AANAT tend to differ even among relatively closely related mammals, let alone other animals (Fig. 1*C*). This pattern of variation suggests a blend of adaptive (function-linked, natural selection-based) changes in N-terminal sequences of AANATs *versus* an unknown (extent-wise) but apparently strong flux of quasi-neutral, drift-mediated changes of these N-terminal sequences on evolutionary time scales.

In the present study, we approached the proteolysis-based regulation of rat and human AANATs (Fig. 1*C*) by expressing them and their mutants not only in mammalian cells but also in the yeast *S. cerevisiae*. This strategy made possible the use of yeast genetics to illuminate specific proteolytic pathways involved, in parallel with experiments in mammalian cells.

We found that the wild-type rat AANAT (^{MLS}rAANAT) is targeted for degradation by two complementary branches of the N-end rule pathway. Specifically, we showed that the Nt-acetylated Ac-^{MLS}rAANAT is destroyed through the recognition of its Nt-acetylated N-terminal Met residue by the Ac/N-end rule pathway, whereas the non-Nt-acetylated ^{MLS}rAANAT is targeted for degradation by the Arg/N-end rule pathway, which recognizes the unacetylated N-terminal Met-Leu sequence of ^{MLS}rAANAT.

The N-terminal sequence of the wild-type human $^{(M)ST}$hAANAT ((Met)-Ser-Thr) is different from the Met-Leu-Ser sequence of rat ^{MLS}rAANAT (Fig. 1*C*). We found that the wild-type human $^{(M)ST}$hAANAT is considerably longer-lived than its rat ^{MLS}rAANAT counterpart and does not appear to be an efficacious N-end rule substrate. Together, these and related results (Figs. 2–7) indicated both a major involvement of the N-end rule pathway in the control of rodent (specifically rat) AANAT and substantial differences in the regulation of rodent and human AANATs that stem from differences in their N-terminal sequences.

The observed co-targeting of the two "complementary" forms of the rat ^{MLS}rAANAT by the two "complementary" branches of the N-end rule pathway (Figs. 2 and 3) is in agreement with the earlier finding that the N-terminal region of ^{MLS}rAANAT, and specifically its Leu-2 residue, are an important determinant of the observed metabolic instability of this AANAT (37). The cited study also suggested that either the Lys residues of ^{MLS}rAANAT or its surface-exposed Cys residues were not essential for its proteasome-mediated degradation (37). In the present work, we compared the degradation of wild-type ^{MLS}rAANAT and its lysine-lacking ^{MLS}rAANAT$^{Kzero}_{3ha}$ mutant using CHX-chases. Our results showed that the C-terminally triple-HA-tagged ^{MLS}rAANAT$^{Kzero}_{3ha}$ mutant was completely stabilized in human HEK293T cells, in contrast to instability of wild-type ^{MLS}rAANAT, indicating that at least some Lys residues of ^{MLS}rAANAT were required for its degradation (Fig. 6, *B* and *D*).

A possible explanation of the above discrepancy stems from different choices of C-terminal epitope tags in the earlier and the present study. Specifically, Huang *et al.* (37) employed ^{MLS}rAANAT C-terminally tagged with c-Myc epitope (EQKLISEEDL), which contains a Lys residue. In the present work, we used a triple-HA tag, which lacks Lys residues (the sequence of

single HA is YPYDVPDYA). Previous analyses of N-degrons have shown that the targeting apparatus of the Arg/N-end rule pathway selects a substrate's internal lysine as a polyubiquitylation site through a process in which different (spatially competing, conformationally mobile) Lys residues can be chosen stochastically, depending on their ability to become transiently close to the substrate-bound E2-E3 complex (41, 51, 86). Thus, the presence of a Lys residue in the C-terminal c-Myc epitope of the earlier study (37) might have rendered the otherwise lysine-lacking ^{MLS}rAANAT mutant still targetable by the N-end rule pathway. Indeed, tellingly, our initial experiments with lysine-lacking mutants of ^{MLS}rAANAT have employed, inadvertently, a lysine-containing C-terminal FLAG tag instead of the lysine-lacking HA tag. Remarkably, the otherwise lysine-lacking but FLAG-tagged ^{MLS}rAANAT$^{Kzero}_{3f}$ mutant was found to be unstable (Figs. 6*B* (*right*) and 7*E*), in contrast to the actually (completely) lysine-lacking, HA-tagged ^{MLS}rAANAT$^{Kzero}_{3ha}$ mutant (Fig. 6, *B* (*left*) and *D*), in agreement with the above tag-based explanation.

In addition to polyubiquitylation and degradation, AANAT is also regulated through a site-specific phosphorylation, a modification that stimulates the binding of AANAT to at least one of the 14-3-3 chaperone-like proteins (they are encoded by a family of several *14-3-3* genes in mammals). This interaction with 14-3-3 both protects (phosphorylated) AANAT from degradation and enhances its catalytic activity. Rat, human, and other AANATs contain two previously mapped phosphorylation sites, Thr-29 and Ser-203 (position numbers refer to the sequence of rat ^{MLS}rAANAT). Phosphorylation at Thr-29 is conserved in all examined mammalian AANATs (31). This phosphorylation, by PKA and/or by PKC, augments the interaction between AANAT and 14-3-3 both *in vitro* and *in vivo* (1, 5, 37). By expressing AANATs not only in mammalian cells but also in the heterologous setting of *S. cerevisiae*, we could analyze the degradation of AANATs in the possible absence of phosphorylation at Thr-29 (or its equivalent) and also in the possible absence of AANAT interactions with 14-3-3 proteins. Whereas *S. cerevisiae* has two 14-3-3 proteins (87), there is no evidence, so far, that bears on their binding, *in vivo*, to a mammalian AANAT.

Our attempts to observe a phosphorylation-induced *in vivo* binding of the wild-type rat ^{MLS}rAANAT either to an endogenous yeast 14-3-3 protein or to the (overexpressed) human 14-3-3ζ protein were unsuccessful so far, despite a variety of tried approaches.[5] Nevertheless, the likely conceptual benefit of achieving a phosphorylation-inducible interaction between a mammalian AANAT and a specific 14-3-3 protein, in a setting of greatly reduced complexity of 14-3-3s (in comparison with the large set of their mammalian counterparts), justifies further work in this direction. 14-3-3 proteins are abundant, broadly expressed, multifunctional chaperone-like proteins that modulate catalytic activities of enzymes to which 14-3-3s bind and also regulate protein-protein interactions and subcellular targeting of specific proteins (88–90). It is possible, indeed likely, that 14-3-3 proteins may bind, in a regulated manner, not only to, for example, rat ^{MLS}rAANAT but to other N-end rule substrates as well, thereby controlling the rates of degradation of such substrates in ways that remain to be explored.

Recently, the naturally occurring mutant human protein RGS2^{Q2L} was shown to be a conditionally short-lived substrate of both the Ac/N-end rule pathway and the Arg/N-end rule pathway (60). This clinically relevant mutant of RGS2 (a negative regulator of specific G proteins) was identified in a cohort of hypertensive Japanese patients (91) (also see the Introduction). In the present study, we demonstrated that the otherwise unrelated rat ^{MLS}rAANAT protein, whose N-terminal Met-Leu sequence is identical to that of RGS2^{Q2L}, is also targeted for degradation by both branches of the N-end rule pathway (Figs. 1 and 2). These results further expanded the set of identified mammalian N-end rule substrates of the Met-Φ type.

Interestingly, RGS2, an N-end rule substrate (60), has been identified as a physiologically relevant inhibitor of the AANAT-dependent melatonin production (92). Light-stimulated, norepinephrine-induced increases in the levels and activity of AANAT are mediated by G-protein-coupled adrenergic receptors, whose activation increases intracellular cAMP, and subsequently the levels of AANAT as well, at least in part through an increased phosphorylation of AANAT and the resulting induction of its binding to protective 14-3-3 proteins (5, 28). While acting to increase the levels and activity of AANAT (which is required for the synthesis of NAS and melatonin), cAMP also acts as a negative feedback inhibitor of melatonin production through up-regulation of *Rgs2* transcription. The resulting increase in RGS2 inhibits the activity of G proteins that are coupled to the norepinephrine-responsive receptor, a negative feedback circuit that acts to decrease cAMP levels (92). AANAT results of the present study, together with the earlier evidence that RGS2 is both a conditionally short-lived N-end rule substrate and an (indirect) down-regulator of AANAT (60, 92), indicate that the N-end rule pathway is a pleiotropic controller of circuits that either directly or indirectly modulate AANAT.

Previous studies of AANAT demonstrated that its transcriptional regulation can be different in different species, but it has been conjectured that mechanisms and regulation of AANAT degradation would be more conserved in evolution (11, 34–36). As shown in the present study, the rates of degradation of the human and rat AANAT proteins are quite different. Moreover, whereas rat ^{MLS}rAANAT is destroyed by the N-end rule pathway (Figs. 2 and 6), human $^{(M)ST}$hAANAT is substantially resistant to this pathway (Figs. 3 and 7). Nevertheless, if the identification of RGS2 as a feedback inhibitor of AANAT expression in the rat pineal gland (92) could also be shown to extend to human RGS2, the N-end rule pathway would be a regulator of AANAT in humans as well, albeit an indirect one.

An earlier study of human $^{(M)ST}$hAANAT described its apparent degradation by the proteasome but did not detect its ubiquitylation (33). In that study, the instability of human $^{(M)ST}$hAANAT was inferred from increases in its steady-state levels in the presence of a proteasome inhibitor. In the present work, we employed, in particular, CHX-chases to show that although human $^{(M)ST}$hAANAT is degraded by the proteasome, it is substantially longer-lived than rat ^{MLS}rAANAT

[5] B. Wadas and A. Varshavsky, unpublished data.

TABLE 1
***S. cerevisiae* strains used in this study**

Strains	Relevant genotypes	Source or reference
BY4742	*MATα his3-1 leu2-0 lys2-0 ura3-0 can1-100*	Open Biosystems
BY15470	*naa30Δ::kanMX6* in BY4742	Open Biosystems
BY10976	*naa10Δ::KanMX6* in BY4742	Open Biosystems
BY17299	*doa10Δ:KanMX6 in BY4742*	Open Biosystems
CHY345	*ubr1Δ::LEU2* in BY4742	Ref. 82
CHY346	*ubr1Δ::LEU2 doa10Δ:KanMX6* in BY4742	This study
BWY29	*naa10Δ::kanMX6 ubr1Δ::LEU2* in BY4742	This study
CHY349	*naa30Δ::kanMX6 ubr1Δ::LEU2* in BY4742	Ref. 40
JOY487	*naa30Δ::natNT2* in BY4742	This study

under the same conditions, either in mammalian cells or in *S. cerevisiae* (Figs. 2–7).

In sum, our results indicate both a major involvement of the N-end rule pathway in the control of rodent AANATs and substantial differences in the regulation of rodent and human AANATs that stem from differences in their N-terminal regions (Fig. 1*C*). What is the cause of the remarkable variability of N-terminal sequences of AANATs during mammalian (and, more generally, animal) evolution? Given the extent of variability (Fig. 1*C*), it is nearly certain that a substantial fraction of these changes resulted from a quasi-neutral, unselected genetic drift (93). At the same time, the broad and biologically relevant variation in detailed circadian rhythms among different animal species (due to specific ecological and physiological adaptations) and the role of AANAT in these rhythms suggest that the seeming randomness of the N-terminal sequences of AANATs (Fig. 1*C*) may be obscuring, so far, a set of adaptive (selected) changes in these sequences over evolutionary time scales.

Experimental Procedures

Yeast Strains, Media, and Genetic Techniques—Standard yeast genetic techniques were used (94–96). *S. cerevisiae* strain BWY29 was constructed by transforming the strain CHY345 (*ubr1*Δ::*LEU2* in the strain background of BY4742) with a PCR-amplified DNA fragment that encoded the selection marker KanMX6 (making cells resistant to kanamycin) and was targeted to the 5′- and 3′-flanking regions of the *NAA10* gene, thereby replacing the ORF of *NAA10* with *KanMX6* (Table 1). *S. cerevisiae* strain JOY487 was made by transforming BY4742 with a PCR-amplified DNA fragment that encoded the natNT2 marker (making cells resistant to nourseothricin) and was targeted to the 5′- and 3′-flanking regions of *PDR5*, thereby replacing the ORF of *PDR5* with *natNT2* (Table 1). The resulting *pdr5*Δ cells were used in experiments that involved the MG132 proteasome inhibitor (Fig. 4, *A* and *B*). Other *S. cerevisiae* strains used in this study were constructed previously and are cited in Table 1. *S. cerevisiae* were transformed using the LiAc/PEG method (97). *S. cerevisiae* media included YPD medium, synthetic complete medium, and synthetic drop-out medium (95, 96).

Plasmids, cDNAs, and Primers—Turbo *Escherichia coli* (New England Biolabs) was used for cloning and maintaining plasmids. Phusion High-Fidelity DNA polymerase (New England Biolabs) was used for carrying out PCR. Nucleotide sequences of all plasmids were verified by DNA sequencing. The plasmids and PCR primers used in this study are described in Tables 2 and 3, respectively.

The low copy pBW105, pBW106, pBW107, and pBW209 plasmids expressed the wild-type rat ^{MLS}rAANAT$_{3f}$ (wild-type rat AANAT bearing the N-terminal sequence Met-Leu-Ser and C-terminally tagged with a triple-FLAG epitope) and its N-terminal mutants $^{(M)SI}$rAANAT$_{3f}$, $^{(M)SMLS}$rAANAT$_{3f}$, and $^{(M)PLS}$rAANAT$_{3f}$, respectively, from the P_{GAL1} promoter. To construct these plasmids, the rat *Aanat* ORF was amplified from pCISII-rAANAT (98), using primers BW2394, BW240, BW241, BW412, BW243, and BW244 (Table 3). The resulting PCR products were digested with EcoRI and HindIII and cloned in EcoRI/HindIII-cut pRS416$_{GAL1}$.

The low copy pBW135 and pBW394 plasmids expressed the wild-type rat ^{MLS}rAANAT C-terminally tagged with the triple-HA epitope (^{MLS}rAANAT$_{3ha}$) and its Lys-8 → Arg mutant ^{MLS}rAANAT$^{K8R}_{3ha}$, respectively, from the P_{CUP1} promoter. To construct these plasmids, the rat *Aanat* ORF was amplified from pCISII-rAANAT (98) using primers BW339, BW704, BW338, BW339, and BW340 (Table 3). The amplified DNA fragments were digested with EcoRI and XhoI and cloned in EcoRI/XhoI-cut pRS313$_{CUP1}$ (59, 99).

The low copy pBW395 and pBW419 plasmids expressed the wild-type human $^{(M)ST}$hAANAT C-terminally tagged with a triple-FLAG epitope ($^{(M)ST}$hAANAT$_{3f}$) and its N-terminal mutant $^{(M)PT}$hAANAT$_{3f}$, respectively, from the P_{GAL1} promoter. To construct these plasmids, the human *AANAT* ORF from Genscript clone OHu55705 (Genscript, Piscataway, NJ) was amplified using primers BW705, BW711, BW712, and BW244 or primers BW771, BW711, BW712, and BW244, respectively (Table 3). The PCR-amplified DNA fragments were digested with EcoRI and HindIII and were ligated into EcoRI/HindIII-cut pRS416$_{GAL1}$ (99). All final DNA constructs were verified by DNA sequencing. See items i–x at the beginning of "Results" for information about rat and human AANAT notations.

For expression of the above AANAT-encoding ORFs in human HEK293T cells, these ORFs were cloned into a modified expression vector derived from pcDNA3. That (modified) vector, termed pcDNA3$_{CMVt1}$, contained a truncated (weakened) version of the P_{CMV} promoter, termed P_{CMVt1}. The pcDNA3$_{CMVt1}$ plasmid was constructed by amplifying, using PCR, the 276-bp fragment that encompassed 104 bp at the 3′-end of the P_{CMV} promoter region in pcDNA3, its T7 promoter site, and its multiple cloning site, using primers BW375 and BW376 (Table 3). The amplified DNA fragment was digested with NruI and XbaI and ligated into NruI/XbaI-cut pcDNA3, yielding the plasmid pBW173 (Table 2). Its truncated P_{CMVt1} promoter retained several proximal promoter elements, including the consensus NFκB site, the CREB-binding site, and two SP1/SP3-binding sites, but lacked more distal enhancer elements. This resulted in a ~70% lower activity of the P_{CMVt1} promoter in HEK293T cells, in comparison with P_{CMV} (Fig. 5, *A–C*).

The pcDNA3$_{CMVt1}$-based plasmids pBW206, pBW211, pBW212, and pBW213 expressed, in HEK293T cells, either the wild-type rat ^{MLS}rAANAT$_{3f}$ or its N-terminal mutants $^{(M)SI}$rAANAT$_{3f}$, $^{(M)SMLS}$rAANAT$_{3f}$, and $^{(M)PLS}$rAANAT$_{3f}$ from the P_{CMVt1} promoter. To construct these plasmids, *Aanat* ORFs were amplified from the plasmids pBW105, pBW106,

TABLE 2
Plasmids used in this study

Plasmid	Description	Source or reference
pcDNA3		Invitrogen
pCISII-rAANAT	rAANAT in pCISII	Ref. 98
pRS313Cup1	pRS313 containing the P_{CUP1} promoter	Varshavsky laboratory collection
pRS416Gal1	pRS416 containing the P_{GAL1} promoter	Varshavsky laboratory collection
pBW105	^{MLS}rAANAT$_{3f}$ in pRS416 with P_{Gal1}	This study
pBW106	$^{(M)SI}$rAANAT$_{3f}$ in pRS416 with P_{Gal1}	This study
pBW107	$^{(M)SMLS}$rAANAT$_{3f}$ in pRS416 with P_{Gal1}	This study
pBW135	^{MLS}rAANAT^{3ha} in pRS313 with P_{Cup1}	This study
pBW173	pcDNA3 (P_{CMVt1})	This study
pBW206	^{MLS}rAANAT$_{3f}$ in pcDNA3 (P_{CMVt1})	This study
pBW209	$^{(M)PLS}$rAANAT$_{3f}$ in pRS416 with P_{Gal1}	This study
pBW211	$^{(M)SMLS}$rAANAT$_{3f}$ in pcDNA3(P_{CMVt1})	This study
pBW212	$^{(M)SI}$rAANAT$_{3f}$ in pcDNA3(P_{CMVt1})	This study
pBW213	$^{(M)PLS}$rAANAT$_{3f}$ in pcDNA3(P_{CMVt1})	This study
pBW394	^{MLS}rAANAT$^{K8R}_{3ha}$ in pRS416 with P_{Gal1}	This study
pBW395	$^{(M)ST}$hAANAT$_{3f}$ in pRS416 with P_{Gal1}	This study
pBW419	$^{(M)PT}$hAANAT$_{3f}$ in pRS416 with P_{Gal1}	This study
pBW466	$^{(M)ST}$hAANAT$_{3f}$ in pcDNA3(P_{CMVt1})	This study
pBW467	$^{(M)PT}$hAANAT$_{3f}$ in pcDNA3(P_{CMVt1})	This study
pBW477	^{MLS}rAANAT$_{3ha}$ in pcDNA3 (P_{CMVt1})	This study
pBW478	^{MLS}rAANAT$^{Kzero}_{3ha}$ in pcDNA3 (P_{CMVt1})	This study
pBW481	$^{(M)ST}$hAANAT$_{3f}$ in pcDNA3(P_{CMVt1})	This study
pBW482	$^{(M)ST}$hAANAT$^{Kzero}_{3ha}$ in pcDNA3(P_{CMVt1})	This study

TABLE 3
PCR primers used in this study

Primer	Sequence
BW239	5′-CCTTGAATTCATACCCATGTTGAGCATCCA-3′
BW240	5′-CCTTGAATTCATACCCATGAGCATCCA-3′
BW241	5′-CCTTGAATTCATACCCATGAGCATGTTGAGCA-3′
BW243	5′-CCTTTCCTTGTAGTCGGATCCACCGCAGCCACTGTT-3′
BW244	5′-CCTTAAGCTTACTTGTCATCGTCGTCCTTGTAGTCGG-3′
BW335	5′-TTGAATTCATGTTGAGCATCCACCCC-3′
BW338	5′-GTATGGGTAGCAGCCACTGTTCC-3′
BW339	5′-CAGTGGCTGCTACCCATACGATG-3′
BW340	5′-TTCTCGAGTCAAGCGTAATCTGGAACGTC-3′
BW352	5′-AATTGAATTCACCATGTTGAGCATCC-3′
BW353	5′-AATTGAATTCACCATGAGCATCCACC-3′
BW354	5′-AATTGAATTCACCATGAGCATGTTGA-3′
BW355	5′-AATTCTCGAGTTACTTGTCATCGTCG-3′
BW375	5′-TTAATCTAGATGCATGCTCGAGC-3′
BW376	5′-CGTTAATCGCGACCAAAATCAACGGGACTTTC-3′
BW412	5′-TTGAATTCATGCCCTTGAGCATCCACCCC-3′
BW705	5′-TTGAATTCATACCCATGTCCACGCAGAGCACCCACCCCCTGAAACCTGA GGCCCCACGTCTGCCACCTGGGATC-3′
BW711	5′-CTTATAGTCACCAGAACCAGAGCAGCCGCTGTTCCTGCGCAGG-3′
BW712	5′-CAGGAACAGCGGCTGCTCTGGTTCTGGTGACTATAAGGATG-3′
BW771	5′-TTGAATTCATACCCATGCCAACGCAGAGCACCCACCCCCTGAAACCTG AGGCCCCACGTCTGCCACCTGGGATC-3′
BW784	5′-CTGAGTAAGTCTCTCTCTGTCCCAAAGTGAACC-3′
BW785	5′-GGTTCACTTTGGGACAGAGAGAGACTTACTCAG-3′
BW786	5′-CAGCAGGACGGAGCCTCTGCCCTGCTGCCGGAAG-3′
BW787	5′-CTTCCGGCAGCAGGGCAGAGGCTCCGTCCTGCTG-3′
BW788	5′-GGCCTGGAAACCAAATCTCTCATAGAAGGGCAC-3′
BW789	5′-GTGCCCTTCTATGAGAGATTTGGTTTCCAGGCC-3′
BW866	5′-TTGAATTCACCATGTCCACGCAGAGCACCCACCCCC-3′
BW867	5′-TTGAATTCACCATGTCCACGCAGAGCACCCACCCCCTGAGACCTGAGGC-3′
BW868	5′-TTGAATTCACCATGCCAACGCAGAGCACCCACCCC-3′
BW884	5′-TTAAGAATTCACCATGTCCACGCAGAGCACC-3′
BW885	5′-GTCAGGAACATCGTATGGGTAGCAGCCGCTGTTCCTGCGCAGG-3′

pBW107, and pBW209 using primers BW352, BW353, BW354, BW413, and BW355, respectively (Table 3). The amplified DNA fragments were digested with EcoRI and XhoI and ligated in EcoRI/XhoI-cut pBW173 (Table 2). All pcDNA3-based constructs designed for expression in HEK293T cells contained the Kozak sequence 5′-ACC immediately upstream of the start codon.

pBW477, which expressed the ^{MLS}rAANAT$_{3ha}$ from the P_{CMVt1} promoter, was constructed by using pBW135 as a PCR template and the primers BW352/BW340. The resulting PCR-amplified DNA fragment was digested with EcoRI and XhoI and ligated into EcoRI/XhoI-cut pBW173 (Table 2). pBW478 expressed ^{MLS}rAANAT$^{Kzero}_{3ha}$ (*i.e.* the lysine-lacking derivative of ^{MLS}rAANAT$_{3ha}$). It was constructed by using pBW135 as a PCR template to generate four separate DNA fragments containing lysine-to-arginine mutations. The primer pairs were 704/784, 785/786, 787/788, and 789/340 (Table 3). These fragments were then assembled into a contiguous ORF using PCR. The resulting DNA fragment, encoding lysine-to-arginine mutations at each of the four lysines contained in the wild-type rat ^{MLS}rAANAT$_{3f}$, was digested with EcoRI and XhoI, and ligated into EcoRI/XhoI-cut pBW173.

pBW466 and pBW467, the pcDNA3-based counterparts of pBW395 and pBW419 (Table 2) were generated by PCR using

pBW395 and pBW419 as templates and the primers BW866/BW355 and BW868/BW355, respectively (Table 3). PCR-amplified DNA fragments were digested with EcoRI and XhoI and ligated into EcoRI/XhoI-cut pBW173 (Table 2).

Cell Culture—The HEK293T cell line (derived from human embryonic kidney cells) was obtained from American Type Culture Collection (ATCC, Manassas, VA) and was grown at 37 °C in 5% CO_2 in DMEM supplemented with 10% FBS (Gemini Bio-Products, West Sacramento, CA) and penicillin/streptomycin (100 units/ml; Hyclone). Cells were transfected using Lipofectamine-2000 (Invitrogen) according to the manufacturer's protocol.

Antibody Specific for the Nt-acetylated Form of Rat AANAT (^{MLS}rAANAT)—Unpurified rabbit polyclonal antisera against the synthetic peptide Ac-MLSIHPLKPEAC were produced by Abgent (San Diego, CA) essentially as described for other peptide-mediated polyclonal antibodies produced in studies by the Varshavsky laboratory (*e.g.* see Refs. 59 and 66). The sequence of the Nt-acetylated peptide immunogen comprised the first 11 residues of ^{MLS}rAANAT (Fig. 1*C*; see below), followed by the C-terminal Cys residue that was used to conjugate the peptide to keyhole limpet hemocyanin carrier protein. The antiserum was affinity-purified in two sequential steps. First, the antibody sample was incubated with the C-terminally immobilized original immunogen Ac-MLSIHPLKPEAC. The peptide-bound fraction was eluted as described previously (59, 66). That fraction was thereafter "negatively" purified against the otherwise identical but non-Nt-acetylated immobilized MLSIHPLKPEAC peptide (the peptides were immobilized using a sulfhydryl-coupling resin (Abgent)), collecting, this time, the unbound fraction. The resulting antibody sample was used to detect, selectively, the Nt-acetylated form of rat AANAT (see "Results" and Fig. 5*D*). The fraction of once purified antibody that was bound to the non-Nt-acetylated MLSIHPLKPEAC peptide was also eluted and retained and was used as an antibody that could recognize the N-terminal region of rat AANAT irrespective of its Nt-acetylation state.

Cycloheximide Chase Assay in S. cerevisiae—CHX-chase assays in *S. cerevisiae* were performed largely as described (39, 59). Briefly, *S. cerevisiae* cells were grown in overnight cultures, and expression of epitope-tagged test proteins was induced by the addition of 2% galactose (for plasmids containing the P_{GAL1} promoter) or 0.1 mM $CuSO_4$ (for plasmids containing the P_{CUP1} promoter (100)). 3 h post-induction, CHX was added to a final concentration of 0.1 mg/ml. Samples were collected at the indicated time points, centrifuged at 11,200 × *g* for 2 min to pellet the cells, and snap-frozen in liquid nitrogen. Proteins were extracted by resuspending the pellets in 1 ml of 0.2 M NaOH and incubating on ice for 20 min (101). Cells were then pelleted and resuspended in 50 μl of SUMEB loading buffer (1% SDS, 8 M urea, 10 mM EDTA, 0.01% bromphenol blue, 10 mM MOPS, pH 6.8), followed by heating at 95 °C for 10 min. Samples were then centrifuged at 11,200 × *g* for 5 min, followed by SDS-PAGE (with 10 μl loaded per well) using 4–12% NuPAGE gels (Invitrogen). Fractionated proteins were transferred onto nitrocellulose membranes for immunoblotting analyses (see below).

Cycloheximide Chase Assay in Mammalian Cell Lines—HEK293T cells were transfected with 4 μg of plasmid DNA per well (10-cm^2 surface area) in 6-well plates using Lipofectamine-2000 (Invitrogen) according to the manufacturer's protocol. 24 h after transfection, cells were treated with CHX (0.1 mg/ml) to initiate a chase. All cells from one well were collected at each indicated time point by washing cells quickly in ice-cold PBS and then rapidly scraping cells into 1.5-ml tubes, pelleting them by centrifugation at 4 °C (at 10,000 × *g* for 1 min), and snap-freezing the pellets in liquid nitrogen. Cells in these samples were later lysed by the addition of 0.2 ml of "mammalian lysis buffer" (1% Nonidet P-40, 0.15 M NaCl, 50 mM Tris-HCl, pH 7.5) containing 1× Roche Complete Protease Inhibitor Mixture and brief sonication, followed by centrifugation at 11,200 × *g* for 10 min. Total protein concentration in the supernatants was measured by the bicinchoninic acid (BCA) assay (Thermo Fisher Scientific). 30 μg of total protein in a thus prepared extract in lithium dodecyl sulfate (LDS)-sample buffer (in a volume of 45 μl) were heated at 70 °C for 10 min, followed by LDS-PAGE on a 4–12% BisTris NuPAGE gel (Invitrogen) and subsequent transfer onto nitrocellulose membranes for immunoblotting.

Immunoblotting—Following electrophoresis, proteins separated by LDS-PAGE or SDS-PAGE, as indicated above, were electroblotted on nitrocellulose membranes by iBlot (Invitrogen; Program 3; 7-min transfer). Membranes were blocked and thereafter incubated with the appropriate primary antibody, followed by LI-COR IRDye-conjugated secondary antibodies. IRDye fluorescence was detected using an Odyssey 9120 system (LI-COR, Lincoln, NE), facilitating quantification of immunoblots. All quantification was done on LI-COR Odyssey software. Antibodies used include anti-FLAG mouse monoclonal antibody (clone M2; 1:2,000 dilution; Sigma-Aldrich), anti-α-tubulin mouse monoclonal antibody (clone B-5-1-2; 1:10,000 dilution; Sigma-Aldrich), anti-HA mouse monoclonal antibody (clone HA-7; 1:2,000 dilution; Sigma-Aldrich), anti-β-actin mouse monoclonal antibody Ab8224 (1:4,000 dilution; Abcam, Cambridge, UK), and anti-14-3-3ζ rabbit monoclonal antibody EPR6379 (1:100,000 dilution; Abcam).

Immunoprecipitation of Polyubiquitylated AANAT—HEK293T cells were transfected with 4 μg of plasmid DNA per well (10-cm^2 surface area) in 6-well plates using Lipofectamine-2000 (Invitrogen) according to the manufacturer's protocol. 24 h after transfection, cells were treated with the proteasome inhibitor MG132 (final concentration of 10 μM; AG Scientific, San Diego, CA) or with an equivalent volume of DMSO in which the 10 mM stock solution of MG132 was made, as indicated. 6 h post-treatment, cells were collected by washing them quickly on a plate in ice-cold PBS and then rapidly scraping cells into 1.5-ml tubes and pelleting them by centrifugation at 4 °C at 10,000 × *g* for 1 min. Pellets were resuspended in 0.1 ml of buffer containing 1% SDS and 50 mM Tris (pH 7.5) and heated at 95 °C for 10 min. After boiling, samples were diluted with 1 ml of buffer TNN (0.5% Nonidet P-40, 0.25 M NaCl, 5 mM EDTA, 50 mM Tris, pH 7.5) containing 1× Roche Complete Protease Inhibitor Mixture, 20 mM *N*-ethylmaleimide (Sigma-Aldrich), and 50 μM PR-619 (LifeSensors, Malvern, PA) as inhibitors of deubiquitylation. 25 μl of anti-HA magnetic beads

were then added to each sample, and samples were incubated at 4 °C overnight, followed by three washes in TNN, 1 wash in 10 mM Tris-HCl, pH 8.5, and elution with 50 μl of 0.1 M glycine, pH 2.0, by incubation at room temperature for 10 min. After elution, the samples were neutralized and then heated at 70 °C in LDS-PAGE sample buffer, followed by LDS-PAGE on a 4–12% NuPAGE gel. Fractionated proteins were then electroblotted onto nitrocellulose membranes. The resulting membranes (containing transferred proteins) were autoclaved as described previously (102) before "downstream" immunoblotting procedures with either anti-HA or anti-ubiquitin antibodies to increase the sensitivity of detection of polyubiquitin chains.

Author Contributions—B. W., A. V., J. B., Z. H., J.-H. O., and C-S. H. designed the experiments. B. W. performed the experiments, with participation by J.-H. O. B. W., A. V., and J. B. wrote the paper. All authors discussed the results and commented on the manuscript.

Acknowledgments—We thank the present and former members of the Varshavsky laboratory, particularly K. Piatkov, for helpful discussions during this study.

References

1. Klein, D. C. (2006) Evolution of the vertebrate pineal gland: the AANAT hypothesis. *Chronobiol. Int.* **23,** 5–20
2. Coon, S. L., and Klein, D. C. (2006) Evolution of arylalkylamine *N*-acetyltransferase: emergence and divergence. *Mol. Cell. Endocrinol.* **252,** 2–10
3. Li, J., You, X., Bian, C., Yu, H., Coon, S. L., and Shi, Q. (2016) Molecular evolution of aralkylamine *N*-acetyltransferase in fish: a genomic survey. *Int. J. Mol. Sci.* **17,** E51
4. Borjigin, J., Zhang, L. S., and Calinescu, A. A. (2012) Circadian regulation of pineal gland rhythmicity. *Mol. Cell. Endocrinol.* **349,** 13–19
5. Choi, B. H., Chae, H. D., Park, T. J., Oh, J., Lim, J., Kang, S. S., Ha, H., and Kim, K. T. (2004) Protein kinase C regulates the activity and stability of serotonin *N*-acetyltransferase. *J. Neurochem.* **90,** 442–454
6. Szewczuk, L. M., Tarrant, M. K., Sample, V., Drury, W. J., 3rd, Zhang, J., and Cole, P. A. (2008) Analysis of serotonin *N*-acetyltransferase regulation in vitro and in live cells using protein semisynthesis. *Biochemistry* **47,** 10407–10419
7. Obsil, T., Ghirlando, R., Klein, D. C., Ganguly, S., and Dyda, F. (2001) Crystal structure of the 14-3-3ζ:serotonin *N*-acetyltransferase complex. a role for scaffolding in enzyme regulation. *Cell* **105,** 257–267
8. Hickman, A. B., Namboodiri, M. A., Klein, D. C., and Dyda, F. (1999) The structural basis of ordered substrate binding by serotonin *N*-acetyltransferase: enzyme complex at 1.8 Å resolution with a bisubstrate analog. *Cell* **97,** 361–369
9. Hickman, A. B., Klein, D. C., and Dyda, F. (1999) Melatonin biosynthesis: the structure of serotonin *N*-acetyltransferase at 2.5 Å resolution suggests a catalytic mechanism. *Mol. Cell* **3,** 23–32
10. Borjigin, J., Wang, M. M., and Snyder, S. H. (1995) Diurnal variation in mRNA encoding serotonin *N*-acetyltransferase in pineal gland. *Nature* **378,** 783–785
11. Coon, S. L., Roseboom, P. H., Baler, R., Weller, J. L., Namboodiri, M. A., Koonin, E. V., and Klein, D. C. (1995) Pineal serotonin *N*-acetyltransferase: expression cloning and molecular analysis. *Science* **270,** 1681–1683
12. Tosini, G., Ye, K., and Iuvone, P. M. (2012) *N*-Acetylserotonin: neuroprotection, neurogenesis, and the sleepy brain. *Neuroscientist* **18,** 645–653
13. Jang, S. W., Liu, X., Pradoldej, S., Tosini, G., Chang, Q., Iuvone, P. M., and Ye, K. (2010) *N*-Acetylserotonin activates TrkB receptor in a circadian rhythm. *Proc. Natl. Acad. Sci. U.S.A.* **107,** 3876–3881
14. Sompol, P., Liu, X., Baba, K., Paul, K. N., Tosini, G., Iuvone, P. M., and Ye, K. (2011) *N*-Acetylserotonin promotes hippocampal neuroprogenitor cell proliferation in sleep-deprived mice. *Proc. Natl. Acad. Sci. U.S.A.* **108,** 8844–8849
15. Schippers, K. J., and Nichols, S. A. (2014) Deep, dark secrets of melatonin in animal evolution. *Cell* **159,** 9–10
16. Zhdanova, I. V., Wang, S. Y., Leclair, O. U., and Danilova, N. P. (2001) Melatonin promotes sleep-like state in zebrafish. *Brain Res.* **903,** 263–268
17. Gandhi, A. V., Mosser, E. A., Oikonomou, G., and Prober, D. A. (2015) Melatonin is required for the circadian regulation of sleep. *Neuron* **85,** 1193–1199
18. González, S., Moreno-Delgado, D., Moreno, E., Pérez-Capote, K., Franco, R., Mallol, J., Cortés, A., Casadó, V., Lluís, C., Ortiz, J., Ferré, S., Canela, E., and McCormick, P. J. (2012) Circadian-related heteromerization of adrenergic and dopamine D(4) receptors modulates melatonin synthesis and release in the pineal gland. *PLoS Biol.* **10,** e1001347
19. Rawashdeh, O., and Maronde, E. (2012) The hormonal Zeitgeber melatonin: role as a circadian modulator in memory processing. *Front. Mol. Neurosci.* **5,** 27
20. Arendt, J. (2006) Melatonin and human rhythms. *Chronobiol. Int.* **23,** 21–37
21. Liu, T., and Borjigin, J. (2005) *N*-Acetyltransferase is not the rate-limiting enzyme of melatonin synthesis at night. *J. Pineal Res.* **39,** 91–96
22. Tu, B. P., and McKnight, S. L. (2006) Metabolic cycles as an underlying basis of biological oscillations. *Nat. Rev. Mol. Cell Biol.* **7,** 696–701
23. Masri, S., and Sassone-Corsi, P. (2013) The circadian clock: a framework linking metabolism, epigenetics and neuronal function. *Nat. Rev. Neurosci.* **14,** 69–75
24. Edgar, R. S., Green, E. W., Zhao, Y., van Ooijen, G., Olmedo, M., Qin, X., Xu, Y., Pan, M., Valekunja, U. K., Feeney, K. A., Maywood, E. S., Hastings, M. H., Baliga, N. S., Merrow, M., Millar, A. J., Johnson, C. H., Kyriacou, C. P., O'Neill, J. S., and Reddy, A. B. (2012) Peroxiredoxins are conserved markers of circadian rhythms. *Nature* **485,** 459–464
25. Borjigin, J., Li, X., and Snyder, S. H. (1999) The pineal gland and melatonin: molecular and pharmacologic regulation. *Annu. Rev. Pharmacol. Toxicol.* **39,** 53–65
26. Stehle, J. H., Saade, A., Rawashdeh, O., Ackermann, K., Jilg, A., Sebestény, T., and Maronde, E. (2011) A survey of molecular details in the human pineal gland in the light of phylogeny, structure, function and chronobiological diseases. *J. Pineal Res.* **51,** 17–43
27. Mohawk, J. A., and Takahashi, J. S. (2011) Cell autonomy and synchrony of suprachiasmatic nucleus circadian oscillators. *Trends Neurosci.* **34,** 349–358
28. Ganguly, S., Gastel, J. A., Weller, J. L., Schwartz, C., Jaffe, H., Namboodiri, M. A., Coon, S. L., Hickman, A. B., Rollag, M., Obsil, T., Beauverger, P., Ferry, G., Boutin, J. A., and Klein, D. C. (2001) Role of a pineal cAMP-operated arylalkylamine *N*-acetyltransferase/14-3-3-binding switch in melatonin synthesis. *Proc. Natl. Acad. Sci. U.S.A.* **98,** 8083–8088
29. Mukherjee, S., and Maitra, S. K. (2015) Gut melatonin in vertebrates: chronobiology and physiology. *Front. Endocrinol.* **6,** 112
30. Hardeland, R. (2010) Melatonin metabolism in the central nervous system. *Curr. Neuropharmacol.* **8,** 168–181
31. Chattoraj, A., Liu, T., Zhang, L. S., Huang, Z., and Borjigin, J. (2009) Melatonin formation in mammals: *in vivo* perspectives. *Rev. Endocr. Metab. Disord.* **10,** 237–243
32. Schomerus, C., Laedtke, E., Olcese, J., Weller, J. L., Klein, D. C., and Korf, H. W. (2002) Signal transduction and regulation of melatonin synthesis in bovine pinealocytes: impact of adrenergic, peptidergic and cholinergic stimuli. *Cell Tissue Res.* **309,** 417–428
33. Schomerus, C., Korf, H. W., Laedtke, E., Weller, J. L., and Klein, D. C. (2000) Selective adrenergic/cyclic AMP-dependent switch-off of proteasomal proteolysis alone switches on neural signal transduction: an example from the pineal gland. *J. Neurochem.* **75,** 2123–2132
34. Bernard, M., Iuvone, P. M., Cassone, V. M., Roseboom, P. H., Coon, S. L., and Klein, D. C. (1997) Avian melatonin synthesis: photic and circadian regulation of serotonin *N*-acetyltransferase mRNA in the chicken pineal gland and retina. *J. Neurochem.* **68,** 213–224
35. Gastel, J. A., Roseboom, P. H., Rinaldi, P. A., Weller, J. L., and Klein, D. C. (1998) Melatonin production: proteasomal proteolysis in serotonin *N*-

acetyltransferase regulation. *Science* **279,** 1358–1360
36. Roseboom, P. H., Coon, S. L., Baler, R., McCune, S. K., Weller, J. L., and Klein, D. C. (1996) Melatonin synthesis: analysis of the more than 150-fold nocturnal increase in serotonin *N*-acetyltransferase messenger ribonucleic acid in the rat pineal gland. *Endocrinology* **137,** 3033–3045
37. Huang, Z., Liu, T., and Borjigin, J. (2010) N-terminal residues regulate proteasomal degradation of AANAT. *J. Pineal Res.* **48,** 290–296
38. Bachmair, A., Finley, D., and Varshavsky, A. (1986) *In vivo* half-life of a protein is a function of its amino-terminal residue. *Science* **234,** 179–186
39. Hwang, C. S., Shemorry, A., and Varshavsky, A. (2010) N-terminal acetylation of cellular proteins creates specific degradation signals. *Science* **327,** 973–977
40. Kim, H. K., Kim, R. R., Oh, J. H., Cho, H., Varshavsky, A., and Hwang, C. S. (2014) The N-terminal methionine of cellular proteins as a degradation signal. *Cell* **156,** 158–169
41. Varshavsky, A. (2011) The N-end rule pathway and regulation by proteolysis. *Protein Sci.* **20,** 1298–1345
42. Gibbs, D. J., Bacardit, J., Bachmair, A., and Holdsworth, M. J. (2014) The eukaryotic N-end rule pathway: conserved mechanisms and diverse functions. *Trends Cell Biol.* **24,** 603–611
43. Tasaki, T., Sriram, S. M., Park, K. S., and Kwon, Y. T. (2012) The N-end rule pathway. *Annu. Rev. Biochem.* **81,** 261–289
44. Dougan, D. A., Micevski, D., and Truscott, K. N. (2012) The N-end rule pathway: from recognition by N-recognins to destruction by AAA+ proteases. *Biochim. Biophys. Acta* **1823,** 83–91
45. Varshavsky, A. (2008) Discovery of cellular regulation by protein degradation. *J. Biol. Chem.* **283,** 34469–34489
46. Lee, K. E., Heo, J. E., Kim, J. M., and Hwang, C. S. (2016) N-terminal acetylation-targeted N-end rule proteolytic system: the Ac/N-end rule pathway. *Mol. Cells* **39,** 169–178
47. Turner, G. C., Du, F., and Varshavsky, A. (2000) Peptides accelerate their uptake by activating a ubiquitin-dependent proteolytic pathway. *Nature* **405,** 579–583
48. Hwang, C. S., Shemorry, A., and Varshavsky, A. (2009) Two proteolytic pathways regulate DNA repair by cotargeting the Mgt1 alkylguanine transferase. *Proc. Natl. Acad. Sci. U.S.A.* **106,** 2142–2147
49. Heck, J. W., Cheung, S. K., and Hampton, R. Y. (2010) Cytoplasmic protein quality control degradation mediated by parallel actions of the E3 ubiquitin ligases Ubr1 and San1. *Proc. Natl. Acad. Sci. U.S.A.* **107,** 1106–1111
50. Eisele, F., and Wolf, D. H. (2008) Degradation of misfolded proteins in the cytoplasm by the ubiquitin ligase Ubr1. *FEBS Lett.* **582,** 4143–4146
51. Bachmair, A., and Varshavsky, A. (1989) The degradation signal in a short-lived protein. *Cell* **56,** 1019–1032
52. Inobe, T., and Matouschek, A. (2014) Paradigms of protein degradation by the proteasome. *Curr. Opin. Struct. Biol.* **24,** 156–164
53. Tobias, J. W., Shrader, T. E., Rocap, G., and Varshavsky, A. (1991) The N-end rule in bacteria. *Science* **254,** 1374–1377
54. Mogk, A., Schmidt, R., and Bukau, B. (2007) The N-end rule pathway of regulated proteolysis: prokaryotic and eukaryotic strategies. *Trends Cell Biol.* **17,** 165–172
55. Rivera-Rivera, I., Román-Hernández, G., Sauer, R. T., and Baker, T. A. (2014) Remodeling of a delivery complex allows ClpS-mediated degradation of N-degron substrates. *Proc. Natl. Acad. Sci. U.S.A.* **111,** E3853–E3859
56. Piatkov, K. I., Vu, T. T., Hwang, C.-S., and Varshavsky, A. (2015) Formylmethionine as a degradation signal at the N-termini of bacterial proteins. *Microbial Cell* **2,** 376–393
57. Humbard, M. A., Surkov, S., De Donatis, G. M., Jenkins, L. M., and Maurizi, M. R. (2013) The N-degradome of *Escherichia coli*: limited proteolysis *in vivo* generates a large pool of proteins bearing N-degrons. *J. Biol. Chem.* **288,** 28913–28924
58. Graciet, E., Hu, R. G., Piatkov, K., Rhee, J. H., Schwarz, E. M., and Varshavsky, A. (2006) Aminoacyl-transferases and the N-end rule pathway of prokaryotic/eukaryotic specificity in a human pathogen. *Proc. Natl. Acad. Sci. U.S.A.* **103,** 3078–3083
59. Shemorry, A., Hwang, C. S., and Varshavsky, A. (2013) Control of protein quality and stoichiometries by N-terminal acetylation and the N-end rule pathway. *Mol. Cell* **50,** 540–551
60. Park, S. E., Kim, J. M., Seok, O. H., Cho, H., Wadas, B., Kim, S. Y., Varshavsky, A., and Hwang, C. S. (2015) Control of mammalian G protein signaling by N-terminal acetylation and the N-end rule pathway. *Science* **347,** 1249–1252
61. Aksnes, H., Hole, K., and Arnesen, T. (2015) Molecular, cellular, and physiological significance of N-terminal acetylation. *Int. Rev. Cell. Mol. Biol.* **316,** 267–305
62. Dörfel, M. J., and Lyon, G. J. (2015) The biological functions of Naa10: from amino-terminal acetylation to human disease. *Gene* **567,** 103–131
63. Starheim, K. K., Gevaert, K., and Arnesen, T. (2012) Protein N-terminal acettyltransferases: when the start matters. *Trends Biochem. Sci.* **37,** 152–161
64. Piatkov, K. I., Brower, C. S., and Varshavsky, A. (2012) The N-end rule pathway counteracts cell death by destroying proapoptotic protein fragments. *Proc. Natl. Acad. Sci. U.S.A.* **109,** E1839–E1847
65. Piatkov, K. I., Oh, J.-H., Liu, Y., and Varshavsky, A. (2014) Calpain-generated natural protein fragments as short-lived substrates of the N-end rule pathway. *Proc. Natl. Acad. Sci. U.S.A.* **111,** E817–E826
66. Brower, C. S., Piatkov, K. I., and Varshavsky, A. (2013) Neurodegeneration-associated protein fragments as short-lived substrates of the N-end rule pathway. *Mol. Cell* **50,** 161–171
67. Yamano, K., and Youle, R. J. (2013) PINK1 is degraded through the N-end rule pathway. *Autophagy* **9,** 1758–1769
68. Cha-Molstad, H., Sung, K. S., Hwang, J., Kim, K. A., Yu, J. E., Yoo, Y. D., Jang, J. M., Han, D. H., Molstad, M., Kim, J. G., Lee, Y. J., Zakrzewska, A., Kim, S. H., Kim, S. T., Kim, S. Y., *et al.* (2015) Amino-terminal arginylation targets endoplasmic reticulum chaperone BiP for autophagy through p62 binding. *Nat. Cell Biol.* **17,** 917–929
69. Wang, H., Piatkov, K. I., Brower, C. S., and Varshavsky, A. (2009) Glutamine-specific N-terminal amidase, a component of the N-end rule pathway. *Mol. Cell* **34,** 686–695
70. Hwang, C. S., Shemorry, A., Auerbach, D., and Varshavsky, A. (2010) The N-end rule pathway is mediated by a complex of the RING-type Ubr1 and HECT-type Ufd4 ubiquitin ligases. *Nat. Cell Biol.* **12,** 1177–1185
71. Varshavsky, A. (2004) Spalog and sequelog: neutral terms for spatial and sequence similarity. *Curr. Biol.* **14,** R181–R183
72. Hassink, G., Kikkert, M., van Voorden, S., Lee, S.-J., Spaapen, R., van Laar, T., Coleman, C. S., Bartee, E., Früh, K., Chau, V., and Wiertz, E. (2005) TEB4 is a C4HC3 RING-finger containing ubiquitin ligase of the endoplasmic reticulum. *Biochem. J.* **388,** 647–655
73. Foresti, O., Ruggiano, A., Hannibal-Bach, H. K., Ejsing, C. S., and Carvalho, P. (2013) Sterol homeostasis requires regulated degradation of squalene monooxygenase by the ubiquitin ligase Doa10/Teb4. *Elife* **2,** e00953
74. Xiao, Q., Zhang, F., Nacev, B. A., Liu, J. O., and Pei, D. (2010) Protein N-terminal processing: substrate specificity of *Escherichia coli* and human methionine aminopeptidases. *Biochemistry* **49,** 5588–5599
75. Varland, S., Osberg, C., and Arnesen, T. (2015) N-terminal modifications of cellular proteins: the enzymes involved, their substrate specificities and biological effects. *Proteomics* **15,** 2385–2401
76. Perrot, M., Massoni, A., and Boucherie, H. (2008) Sequence requirements for N^{α}-terminal acetylation of yeast proteins by NatA. *Yeast* **25,** 513–527
77. Lee, D. H., and Goldberg, A. L. (1996) Selective inhibitors of the proteasome-dependent and vacuolar pathways of protein degradation in *Saccharomyces cerevisiae*. *J. Biol. Chem.* **271,** 27280–27284
78. Fleming, J. A., Lightcap, E. S., Sadis, S., Thoroddsen, V., Bulawa, C. E., and Blackman, R. K. (2002) Complementary whole-genome technologies reveal the cellular response to proteasome inhibition by PS-341. *Proc. Natl. Acad. Sci. U.S.A.* **99,** 1461–1466
79. Lee, S. J., Liu, T., Chattoraj, A., Zhang, S. L., Wang, L., Lee, T. M., Wang, M. M., and Borjigin, J. (2009) Posttranscriptional regulation of pineal melatonin synthesis in Octodon degus. *J. Pineal Res.* **47,** 75–81
80. Falcón, J., Coon, S. L., Besseau, L., Cazaméa-Catalan, D., Fuentès, M., Magnanou, E., Paulin, C. H., Boeuf, G., Sauzet, S., Jørgensen, E. H., Mazan, S., Wolf, Y. I., Koonin, E. V., Steinbach, P. J., Hyodo, S., and Klein,

D. C. (2014) Drastic neofunctionalization associated with evolution of the timezyme AANAT 500 Mya. *Proc. Natl. Acad. Sci. U.S.A.* **111,** 314–319
81. Ganguly, S., Mummaneni, P., Steinbach, P. J., Klein, D. C., and Coon, S. L. (2001) Characterization of the *Saccharomyces cerevisiae* homolog of the melatonin rhythm enzyme arylalkylamine *N*-acetyltransferase. *J. Biol. Chem.* **276,** 47239–47247
82. Kim, J. M., and Hwang, C. S. (2014) Crosstalk between the Arg/N-end and Ac/N-end rule. *Cell Cycle* **13,** 1366–1367
83. Slater, M., Hartzell, D., Hartnett, J., Wheeler, S., Stecha, P., and Karassina, N. (2008) Achieve the protein expression level you need with the mammalian HaloTag 7 Flexi vectors. *Promega Notes* **100,** 16–18
84. Wu, C., and Li, S. S. (2009) CelluSpots: a reproducible means of making peptide arrays for the determination of SH2 domain binding specificity. *Methods Mol. Biol.* **570,** 197–202
85. Komander, D., and Rape, M. (2012) The ubiquitin code. *Annu. Rev. Biochem.* **81,** 203–229
86. Inobe, T., Fishbain, S., Prakash, S., and Matouschek, A. (2011) Defining the geometry of the two-component proteasome degron. *Nat. Chem. Biol.* **7,** 161–167
87. van Heusden, G. P., and Steensma, H. Y. (2006) Yeast 14-3-3 proteins. *Yeast* **23,** 159–171
88. Obsil, T., and Obsilova, V. (2011) Structural basis of 14-3-3 protein functions. *Semin. Cell Dev. Biol.* **22,** 663–672
89. Kakiuchi, K., Yamauchi, Y., Taoka, M., Iwago, M., Fujita, T., Ito, T., Song, S. Y., Sakai, A., Isobe, T., and Ichimura, T. (2007) Proteomic analysis of *in vivo* 14-3-3 interactions in the yeast *Saccharomyces cerevisiae*. *Biochemistry* **46,** 7781–7792
90. Obsilova, V., Kopecka, M., Kosek, D., Kacirova, M., Kylarova, S., Rezabkova, L., and Obsil, T. (2014) Mechanisms of the 14-3-3 protein function: regulation of protein function through conformational modulation. *Physiol. Res.* **63,** Suppl. 1, S155–S164
91. Yang, J., Kamide, K., Kokubo, Y., Takiuchi, S., Tanaka, C., Banno, M., Miwa, Y., Yoshii, M., Horio, T., Okayama, A., Tomoike, H., Kawano, Y., and Miyata, T. (2005) Genetic variations of regulator of G-protein signaling 2 in hypertensive patients and in the general population. *J. Hypertens.* **23,** 1497–1505
92. Matsuo, M., Coon, S. L., and Klein, D. C. (2013) RGS2 is a feedback inhibitor of melatonin production in the pineal gland. *FEBS Lett.* **587,** 1392–1398
93. Lynch, M. (2007) *The Origins of Genome Architecture*, Sinauer Associates, Inc., Sunderland, MA
94. Ausubel, F. M., Brent, R., Kingston, R. E., Moore, D. D., Smith, J. A., Seidman, J. G., and Struhl, K. (2010) *Current Protocols in Molecular Biology*, Wiley-Interscience, New York
95. Guthrie, C., and Fink, G. R. (1991) Guide to yeast genetics and molecular biology. *Methods Enzymol.* **194,** 1–863
96. Andrews, B., Boone, C., Davis, T. N., and Fields, S. (2016) *Budding Yeast: A Laboratory Manual*, Cold Spring Harbor Press, Cold Spring Harbor, NY
97. Gietz, R. D., and Woods, R. A. (2002) Transformation of yeast by lithium acetate/single-stranded carrier DNA/polyethylene glycol method. *Methods Enzymol.* **350,** 87–96
98. Huang, Z., Deng, J., and Borjigin, J. (2005) A novel H28Y mutation in LEC rats leads to decreased NAT protein stability *in vivo* and *in vitro*. *J. Pineal Res.* **39,** 84–90
99. Sikorski, R. S., and Hieter, P. (1989) A system of shuttle vectors and yeast host strains designed for efficient manipulation of DNA in *S. cerevisiae*. *Genetics* **122,** 19–27
100. Ghislain, M., Dohmen, R. J., Levy, F., and Varshavsky, A. (1996) Cdc48p interacts with Ufd3p, a WD repeat protein required for ubiquitin-mediated proteolysis in *Saccharomyces cerevisiae*. *EMBO J.* **15,** 4884–4899
101. Kushnirov, V. V. (2000) Rapid and reliable protein extraction from yeast. *Yeast* **16,** 857–860
102. Swerdlow, P. S., Finley, D., and Varshavsky, A. (1986) Enhancement of immunoblot sensitivity by heating of hydrated filters. *Anal. Biochem.* **156,** 147–153

Degradation of Serotonin *N*-Acetyltransferase, a Circadian Regulator, by the N-end Rule Pathway

Brandon Wadas, Jimo Borjigin, Zheping Huang, Jang-Hyun Oh, Cheol-Sang Hwang and Alexander Varshavsky

J. Biol. Chem. 2016, 291:17178-17196.
doi: 10.1074/jbc.M116.734640 originally published online June 23, 2016
